Chapter 7

Transmission-line-matrix Method

"Those who are quite satisfied sit still and do nothing; those who are not quite satisfied are the sole benefactors of the world."   Walter S. Landor

7.1   Introduction

The link between field theory and circuit theory has been exploited in developing numerical techniques to solve certain types of partial differential equations arising in field problems with the aid of equivalent electrical networks [1]. There are three ranges in the frequency spectrum for which numerical techniques for field problems in general have been developed. In terms of the wavelength λ and the approximate dimension ℓ of the apparatus, these ranges are [2]:

$$\lambda >> \ell$$
$$\lambda \approx \ell$$
$$\lambda << \ell$$

In the first range, the special analysis techniques are known as *circuit theory;* in the second, as *microwave theory;* and in the third, as *geometric optics* (frequency independent). Hence the fundamental laws of circuit theory can be obtained from Maxwell's equations by applying an approximation valid when $\lambda >> \ell$. However, it should be noted that circuit theory was not developed by approximating Maxwell's equations, but rather was developed independently from experimentally obtained laws. The connection between circuit theory and Maxwell equations (summarizing field theory) is important; it adds to the comprehension of the fundamentals of electromagnetics. According to Silvester and Ferrari, circuits are mathematical abstractions of physically real fields; nevertheless, electrical engineers at times feel they understand circuit theory more clearly than fields [3].

The idea of replacing a complicated electrical system by a simple equivalent circuit goes back to Kirchhoff and Helmholtz. As a result of Park's [4], Kron's [5, 6] and Schwinger's [7, 8] works, the power and flexibility of equivalent circuits become more
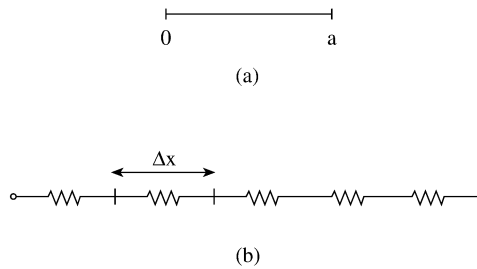
Figure 7.1
(a) One-dimensional conducting system, (b) discretized equivalent.

obvious to engineers. The recent applications of this idea to scattering problems, originally due to Johns [9], has made the method more popular and attractive.

Transmission-line modeling (TLM), otherwise known as the *transmission-line-matrix method,* is a numerical technique for solving field problems using circuit equivalent. It is based on the equivalence between Maxwell's equations and the equations for voltages and currents on a mesh of continuous two-wire transmission lines. The main feature of this method is the simplicity of formulation and programming for a wide range of applications [10, 11]. As compared with the lumped network model, the transmission-line model is more general and performs better at high frequencies where the transmission and reflection properties of geometrical discontinuities cannot be regarded as lumped [7].

Like other numerical techniques, the TLM method is a discretization process. Unlike other methods such as finite difference and finite element methods, which are mathematical discretization approaches, the TLM is a physical discretization approach. In the TLM, the discretization of a field involves replacing a continuous system by a network or array of lumped elements. For example, consider the one-dimensional system (a conducting wire) with no energy storage as in Fig. 7.1(a). The wire can be replaced by a number of lumped resistors providing a discretized equivalent in Fig. 7.1(b). The discretization of the two-dimensional, distributed field is show in Fig. 7.2. More general systems containing energy-reservoir elements as well as dissipative elements will be considered later.

The TLM method involves dividing the solution region into a rectangular mesh of transmission lines. Junctions are formed where the lines cross forming impedance discontinuities. A comparison between the transmission-line equations and Maxwell's equations allows equivalences to be drawn between voltages and currents on the lines and electromagnetic fields in the solution region. Thus, the TLM method involves two basic steps [12]:

- Replacing the field problem by the equivalent network and deriving analogy between the field and network quantities.

- Solving the equivalent network by iterative methods.
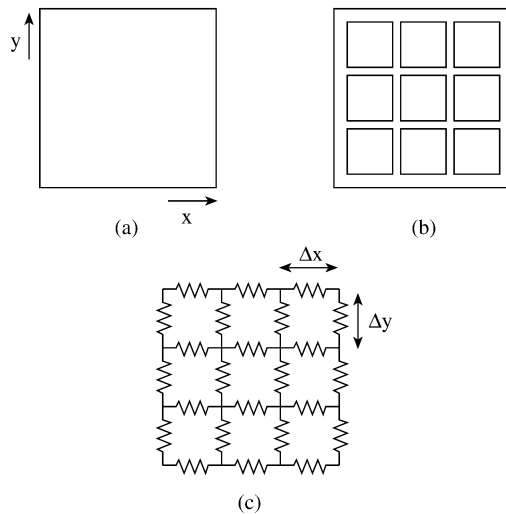
Figure 7.2

(a) Two-dimensional conductive sheet, (b) partially discretized equivalent, (c) fully discretized equivalent.

Before we apply the method, it seems fit to briefly review the basic concepts of transmission lines and then show how the TLM method can be applied to a wide range of EM-related problems.

7.2 Transmission-line Equations

Consider an elemental portion of length $\Delta \ell$ of a two-conductor transmission line. We intend to find an equivalent circuit for this line and derive the line equations. An equivalent circuit of a portion of the line is shown in Fig. 7.3, where the line parameters, R, L, G, and C are resistance per unit length, inductance per unit length, conductance per unit length, and capacitance per unit length of the line, respectively. The model in Fig. 7.3 may represent any two-conductor line. The model is called the T-type equivalent circuit; other types of equivalent circuits are possible, but we end up with the same set of equations. In the model of Fig. 7.3, we assume without loss of generality that wave propagates in the $+z$ direction, from the generator to the load.

By applying Kirchhoff's voltage law to the left loop of the circuit in Fig 7.3, we obtain

$$V(z, t) = R \frac{\Delta \ell}{2} I(z, t) + L \frac{\Delta \ell}{2} \frac{\partial I}{\partial t}(z, t) + V(z + \Delta \ell/2, t)$$
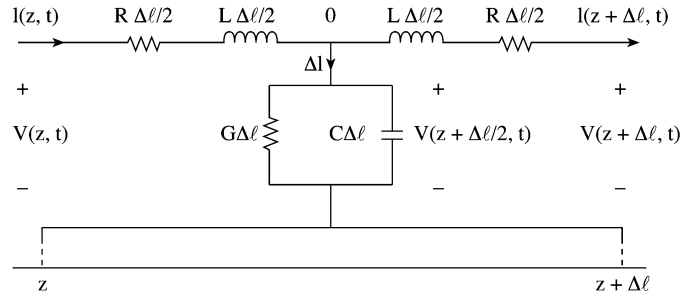
Figure 7.3
T-type equivalent circuit model of a differential length of a two conductor transmission line.

or

$$-\frac{V(z + \Delta\ell/2, t) - V(z, t)}{\Delta\ell/2} = RI(z, t) + L\frac{\partial I}{\partial t}(z, t) \tag{7.1}$$

Taking the limit of Eq. (7.1) as $\Delta\ell \to 0$ leads to

$$-\frac{\partial V(z, t)}{\partial z} = R\,I(z, t) + L\frac{\partial I}{\partial t}(z, t) \tag{7.2}$$

Similarly, applying Kirchhoff's current law to the main node of the circuit in Fig. 7.3 gives

$$I(z, t) = I(z + \Delta\ell, t) + \Delta I$$
$$= I(z + \Delta\ell, t) + G\Delta\ell V(z + \Delta\ell/2, t) + C\Delta\ell\frac{\partial V}{\partial t}(z + \Delta\ell/2, t)$$

or

$$-\frac{I(z + \Delta\ell, t) - I(z, t)}{\Delta\ell} = GV(z + \Delta\ell/2, t) + C\frac{\partial V}{\partial t}(z + \Delta\ell/2, t) \tag{7.3}$$

As $\Delta\ell \to 0$, Eq. (7.3) becomes

$$-\frac{\partial I}{\partial z}(z, t) = GV(z, t) + C\frac{\partial V}{\partial t}(z, t) \tag{7.4}$$

Differentiating Eq. (7.2) with respect to z and Eq. (7.4) with respect to t, the two equations become

$$-\frac{\partial^2 V}{\partial z^2} = R\frac{\partial I}{\partial z} + L\frac{\partial^2 I}{\partial z\,\partial t} \tag{7.2a}$$

and

$$-\frac{\partial^2 I}{\partial t\,\partial z} = G\frac{\partial V}{\partial t} + C\frac{\partial^2 V}{\partial t^2} \tag{7.4a}$$

Substituting Eqs. (7.4) and (7.4a) into Eq. (7.2a) gives

$$\frac{\partial^2 V}{\partial z^2} = LC\frac{\partial^2 V}{\partial t^2} + (RC + GL)\frac{\partial V}{\partial t} + RGV \tag{7.5}$$

Similarly, we obtain the equation for current I as

$$\frac{\partial^2 I}{\partial z^2} = LC\frac{\partial^2 I}{\partial t^2} + (RC + GL)\frac{\partial I}{\partial t} + RGI \tag{7.6}$$

Equations (7.5) and (7.6) have the same mathematical form, which in general may be written as

$$\frac{\partial^2 \Phi}{\partial z^2} = LC\frac{\partial^2 \Phi}{\partial t^2} + (RC + GL)\frac{\partial \Phi}{\partial t} + RG\Phi \tag{7.7}$$

where $\Phi(z, t)$ has replaced either $V(z, t)$ or $I(z, t)$.

Ignoring certain transmission-line parameters in Eq. (7.7) leads to the following special cases [13]:

(a) $L = C = 0$ yields

$$\frac{\partial^2 \Phi}{\partial z^2} = k_1 \Phi \tag{7.8}$$

where $k_1 = RG$. Equation (7.8) is the one-dimensional elliptic partial differential equation called Poisson's equation.

(b) $R = C = 0$ or $G = L = 0$ yields

$$\frac{\partial^2 \Phi}{\partial z^2} = k_2 \frac{\partial \Phi}{\partial t} \tag{7.9}$$

where $k_2 = GL$ or RC. Equation (7.9) is the one-dimensional parabolic partial differential equation called the diffusion equation.

(c) $R = G = 0$ (lossless line) yields

$$\frac{\partial^2 \Phi}{\partial z^2} = k_3 \frac{\partial^2 \Phi}{\partial t^2} \tag{7.10}$$

where $k_3 = LC$. This is the one-dimensional hyperbolic partial differential equation called the Helmholtz equation, or simply the wave equation. Thus, under certain conditions, the one-dimensional transmission line can be used to model problems involving an elliptic, parabolic, or hyperbolic partial differential equation (PDE). The transmission line of Fig. 7.3 reduces to those in Fig. 7.4 for these three special cases.
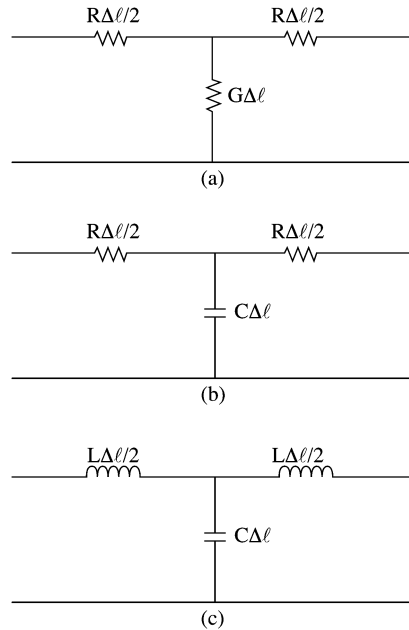
Figure 7.4
Transmission-line equivalent models for: (a) elliptic PDE, Poisson's equation, (b) parabolic PDE, diffusion equation, (c) hyperbolic PDE, wave equation.

Apart from the equivalent models, other transmission-line parameters are of interest. A detailed explanation of these parameters can be found in standard field theory texts, e.g., [14]. We briefly present these important parameters. For the lossless line in Fig. 7.4(c), the characteristic resistance

$$R_o = \sqrt{\frac{L}{C}} \, , \tag{7.11a}$$

the wave velocity

$$u = \frac{1}{\sqrt{LC}} \, , \tag{7.11b}$$

and the reflection coefficient at the load

$$\Gamma = \frac{R_L - R_o}{R_L + R_o} \, , \tag{7.11c}$$

where R_L is the load resistance.

The generality of the TLM method has been demonstrated in this section. In the following sections, the method is applied specifically to diffusion [15, 16] and wave propagation problems [10]–[13], [17, 18].

7.3   Solution of Diffusion Equation

We now apply the TLM method to the diffusion problem arising from current density distribution within a wire [15]. If the wire has a circular cross section with radius a and is infinitely long, then the problem becomes one-dimensional. We will assume sinusoidal source or harmonic fields (with time factor $e^{j\omega t}$).

The analytical solution of the problem has been treated in Example 2.3. For the TLM solution, consider the equivalent network of the cylindrical problem in Fig. 7.5, where $\Delta\ell$ is the distance between nodes or the mesh size. Applying Kirchhoff's laws to the network in Fig. 7.5 gives

$$\frac{\partial I_\rho}{\partial \rho} = -j\omega C V_\phi \tag{7.12a}$$

$$\frac{\partial V_\phi}{\partial \rho} = -R I_\rho \tag{7.12b}$$

where R and C are the resistance and capacitance per unit length.
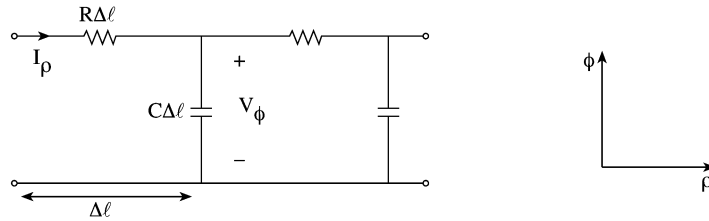
Figure 7.5
RC equivalent network.

Within the conductor, Maxwell's curl equations ($\sigma >> \omega\epsilon$) are

$$\nabla \times \mathbf{E} = -j\omega\mu\mathbf{H} \tag{7.13a}$$

$$\nabla \times \mathbf{H} = \sigma\mathbf{E} \tag{7.13b}$$

where $\mathbf{E}$ and $\mathbf{H}$ are assumed to be in phasor forms. In cylindrical coordinates, Eq. (7.13) becomes

$$-\frac{\partial E_z}{\partial \rho} = -j\omega\mu H_\phi$$

$$\frac{1}{\rho}\frac{\partial}{\partial \rho}(\rho H_\phi) = \sigma E_z$$

These equations can be written as

$$\frac{\partial E_z}{\partial \rho} = j\omega(\mu/\rho)\left(\rho H_\phi\right) \tag{7.14a}$$

$$\frac{\partial}{\partial \rho}\left(\rho H_\phi\right) = (\sigma\rho)E_z \tag{7.14b}$$

Comparing Eq. (7.12) with Eq. (7.14) leads to the following analogy between the network and field quantities:

$$I_\rho \equiv -E_z \tag{7.15a}$$
$$V_\phi \equiv \rho H_\phi \tag{7.15b}$$
$$C \equiv \mu/\rho \tag{7.15c}$$
$$R \equiv \sigma\rho \tag{7.15d}$$

Therefore, solving the impedance network is equivalent to solving Maxwell's equations.
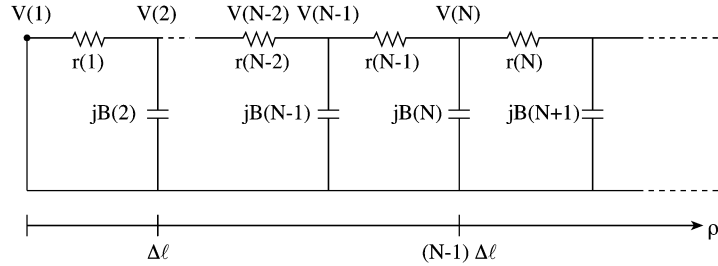
Figure 7.6
The overall equivalent network.

We can solve the overall impedance network in Fig. 7.6 by an iterative method. Since the network in Fig. 7.6 is in the form of a ladder, we apply the *ladder* method. By applying Kirchhoff's current law, the Nth nodal voltage ($N > 2$) is related to $(N-1)$th and $(N-2)$th voltages according to

$$\begin{aligned}
V(N) &= \frac{r(N-1)}{r(N-2)}[V(N-1) - V(N-2)] \\
&\quad + jB(N-1)r(N-1)V(N-1) + V(N-1)
\end{aligned} \tag{7.16}$$

where the resistance r and susceptance B are given by

$$r(N) = R\Delta\ell = \sigma(N - 0.5)(\Delta\ell)^2 \,, \tag{7.17a}$$

$$B(N) = \omega C \Delta\ell = \frac{\omega\mu\Delta\ell}{(N-1)\Delta\ell} = \frac{\omega\mu}{N-1} \tag{7.17b}$$

We note that $V(1) = 0$ because the magnetic field at the center of the conductor ($\rho = 0$) is zero. Also $V(2) = I(1) \cdot r(1)$, where $I(1)$ can be arbitrarily chosen, say $I(1) = 1$. Once $V(1)$ and $V(2)$ are known, we can use Eq. (7.16) to scan all nodes in Fig. 7.6 once from left to right to determine all nodal voltages ($\equiv \rho H_\phi$) and currents ($\equiv E_z = J_z/\sigma$).

Example 7.1

Develop a computer program to determine the relative (or normalized) current density $J_z(\rho)/J_z(a)$ in a round copper wire operated at 1 GHz. Plot the relative current density against the radical position ρ/a for cases $a/\delta = 1, 2,$ and 4. Take $\Delta\ell/\delta = 0.1$, $\mu = \mu_0, \sigma = 5.8 \times 10^7$ mhos/m. ⬚

Solution

The computer program is presented in Fig. 7.7. It calculates the voltage at each node using Eqs. (7.16) and (7.17). The current on each $r(N)$ is found from Fig. 7.6 as

$$I(N-1) = \frac{V(N) - V(N-1)}{r(N-1)}$$

Since $J = \sigma E$, we obtain $J_z(\rho)/J_z(a)$ as the ratio of $I(N)$ and $I(NMAX)$, where $I(NMAX)$ is the current at $\rho = a$.

To verify the accuracy of the TLM solution, we also calculate the exact $J_z(\rho)/J_z(a)$ using Eq. (2.120). (For further details, see Example 2.3.) Table 7.1 shows a comparison between TLM results and exact results for the case $a/\delta = 4.0$. It is noticed that the percentage error is maximum (about 8%) at the center of the wire and diminishes to zero as we approach the surface of the wire. Figure 7.8 portrays the plot of the relative current density versus the radial position for cases $a/\delta = 1, 2,$ and 4. ▮

Table 7.1 Comparison of Relative Current Density Obtained from TLM and Exact Solutions ($a/\delta = 4.0$)

Radial position (ρ/a)	TLM result	Exact result
0.1	0.11581	0.10768
0.2	0.11765	0.11023
0.3	0.12644	0.12077
0.4	0.14953	0.14612
0.5	0.19301	0.19138
0.6	0.26150	0.26082
0.7	0.36147	0.36115
0.8	0.50423	0.50403
0.9	0.70796	0.70786
1.0	1.0	1.0

```
0001    C=====================================================================
0002    C USING THE TLM METHOD, THIS PROGRAM CALCULATES THE RELATIVE
0003    C CURRENT DENSITY JR IN A ROUND COPPER WIRE
0004    C THE EXACT SOLUTION JRE IS ALSO INCLUDED
0005    C=====================================================================
0006
0007            REAL MIU, JR(50), JRE(50)
0008            COMPLEX J, V(50), I(50)
0009            DIMENSION BERO(50), BEIO(50)
0010    C
0011    C FUNCTIONS FOR RESISTANCE AND SUSCEPTANCE
0012    C
0013            R(N) = SIGMA*( FLOAT(N) - 0.5 )*(H**2)
0014            B(N) = OMEGA*MIU/FLOAT(N-1)
0015    C
0016    C SPECIFY INPUT DATA
0017    C
0018            F = 1.0E+9
0019            SIGMA = 5.8E+7
0020            PIE = 4.0*ATAN(1.0)
0021            MIU = 4.0*PIE*1.0E-7
0022            OMEGA = 2.0*PIE*F
0023            DELTA = SQRT( 2.0/( SIGMA*MIU*OMEGA ) )
0024            H = 0.1*DELTA
0025            A = 4.0*DELTA
0026            NMAX = A/H
0027            J = (0.0,1)
0028    C
0029    C INITIALIZE AND CALCULATE RELATIVE CURRENT DENSITY JR
0030    C USING TLM
0031    C
0032            I(1) = (0.1, 0.0)
0033            V(1) = (0.0,0.0)
0034            V(2) = I(1)*R(1)
0035            DO 10  N = 3,NMAX + 1
0036            V(N) = ( R(N-1)/R(N-2) )*( V(N-1) - V(N-2) )
0037       1             + J*B(N-1)*R(N-1)*V(N-1)   +   V(N-1)
0038    10      CONTINUE
0039            I(NMAX) = ( V(NMAX+1) - V(NMAX) )/R(NMAX)
0040            DO 20 N = 2,NMAX + 1
0041            I(N-1) = ( V(N) - V(N-1) )/R(N-1)
0042            JR(N-1) = CABS( I(N-1)/I(NMAX) )
0043    20      CONTINUE
0044    C
0045    C CALCULATE THE CURRENT DENSITY JRE
0046    C FROM THE EXACT SOLUTION
0047    C
0048            DO 40 NRO = 1,NMAX
0049            BERO(NRO) = 0.0
0050            BEIO(NRO) = 0.0
0051            X = ( FLOAT(NRO)/FLOAT(NMAX) )*A*SQRT(2.0)/DELTA
0052            DO 30 K=0,20
0053            CALL FACTORIAL(K,FA)
0054            FB = ( (X/2.0)**(2*K) )/(FA**2)
0055            BERO(NRO) = BERO(NRO) + FB*COS(K*PIE/2.0)
0056            BEIO(NRO) = BEIO(NRO) + FB*SIN(K*PIE/2.0)
0057    30      CONTINUE
0058            JRE(NRO) = SQRT( BERO(NRO)**2 + BEIO(NRO)**2 )
0059    40      CONTINUE
0060            WRITE(6,50)
```

Figure 7.7

Computer program for Example 7.1 *(Continued)*.

```
0061    50      FORMAT(3X,'RADIAL POSITION',4X,'TLM J',12X,'EXACT J',/)
0062            DO 70 N=2,NMAX
0063            RHO = FLOAT(N)/FLOAT(NMAX)
0064            JRE(N) = JRE(N)/JRE(NMAX)     ! RELATIVE CURRENT DENSITY
0065            WRITE(6,60) RHO, JR(N), JRE(N)
0066    60      FORMAT(6X,F5.2,8X,F9.5,8X,F9.5,/)
0067    70      CONTINUE
0068            STOP
0069            END

0001    C ***************************************************
0002    C SUBROUTINE FOR CALCULATE K!
0003    C
0004     SUBROUTINE FACTORIAL(K,F)
0005
0006            F = 1.0
0007            IF(K.GE.2) THEN
0008            DO 10 J = 2,K
0009            F = F*FLOAT(J)
0010    10      CONTINUE
0011            ENDIF
0012            RETURN
0013            END
```

Figure 7.7

(Cont.) **Computer program for Example 7.1.**

7.4 Solution of Wave Equations

In order to show how Maxwell's equations may be represented by the transmission-line equations, the differential length of the lossless transmission line between two nodes of the mesh is represented by lumped inductors and capacitors as shown in Fig. 7.9 for two-dimensional wave propagation problems [17, 18]. At the nodes, pairs of transmission lines form impedance discontinuity. The complete network of transmission-line-matrix is made up of a large number of such building blocks as depicted in Fig. 7.10. Notice that in Fig. 7.10 single lines are used to represent a transmission-line pair. Also, a uniform internodal distance of $\Delta\ell$ is assumed throughout the matrix (i.e., $\Delta\ell = \Delta x = \Delta z$). We shall first derive equivalences between network and field quantities.

7.4.1 Equivalence Between Network and Field Parameters

We refer to Fig. 7.9 and apply Kirchhoff's current law at node O to obtain

$$I_x(x - \Delta\ell/2) - I_x(x + \Delta\ell/2) + I_z(z - \Delta\ell/2) - I_z(z + \Delta\ell/2) = 2C\Delta\ell\frac{\partial V_y}{\partial t}$$

Dividing through by $\Delta\ell$ gives

$$\frac{I_x(x - \Delta\ell/2) - I_x(x + \Delta\ell/2)}{\Delta\ell} + \frac{I_z(z - \Delta\ell/2) - I_z(z + \Delta\ell/2)}{\Delta\ell} = 2C\frac{\partial V_y}{\partial t}$$
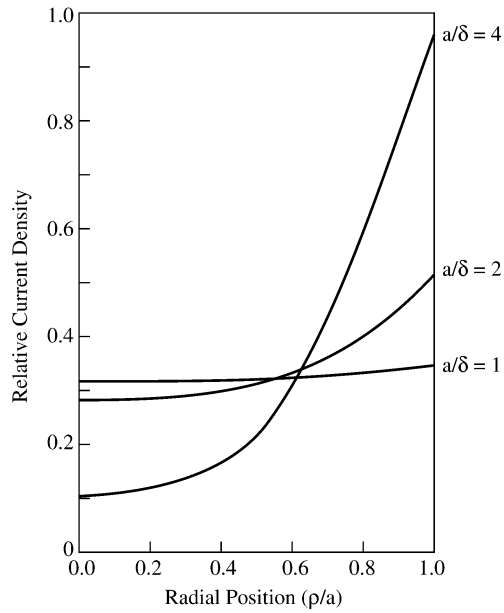
Figure 7.8
**Relative current density versus radial position.**
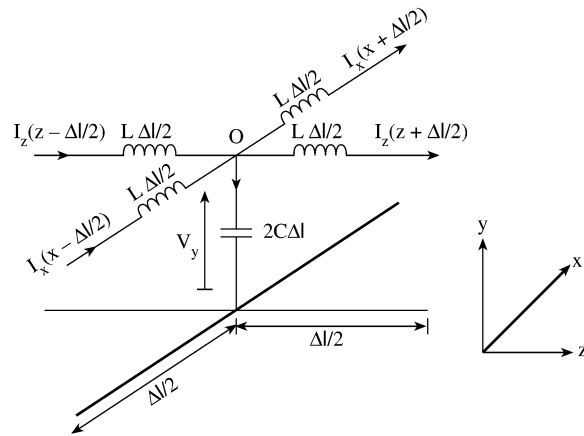
Figure 7.9
**Equivalent network of a two-dimensional TLM shunt node.**
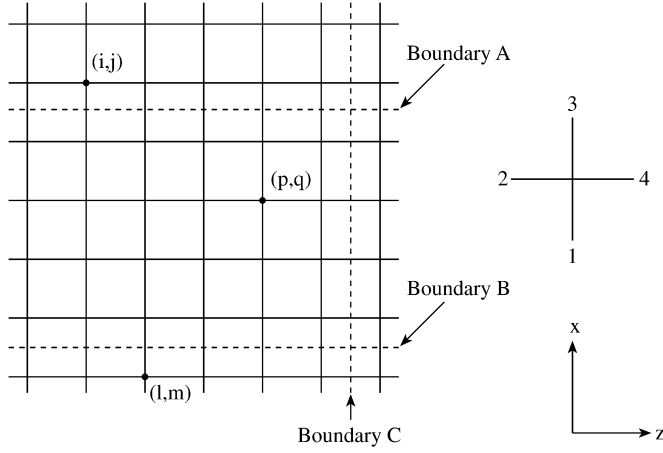
Figure 7.10
Transmission-line matrix and boundaries.

Taking the limit as $\Delta\ell \to 0$ results in

$$-\frac{\partial I_z}{\partial z} - \frac{\partial I_x}{\partial x} = 2C\frac{\partial V_y}{\partial t} \tag{7.18a}$$

Applying Kirchhoff's voltage law around the loop in the $x - y$ plane gives

$$V_y(x - \Delta\ell/2) - L\Delta\ell/2\frac{\partial I_x(x - \Delta\ell/2)}{\partial t}$$
$$-L\Delta\ell/2\frac{\partial I_x(x + \Delta\ell/2)}{\partial t} - V_y(x + \Delta\ell/2) = 0$$

Upon rearranging and dividing by $\Delta\ell$, we have

$$\frac{V_y(x - \Delta\ell/2) - V_y(x + \Delta\ell/2)}{\Delta\ell} = \frac{L}{2}\frac{\partial I_x(x - \Delta\ell/2)}{\partial t} + \frac{L}{2}\frac{\partial I_x(x + \Delta\ell/2)}{\partial t}$$

Again, taking the limit as $\Delta\ell \to 0$ gives

$$\frac{\partial V_y}{\partial x} = -L\frac{\partial I_x}{\partial t} \tag{7.18b}$$

Taking similar steps on the loop in the $y - z$ plane yields

$$\frac{\partial V_y}{\partial z} = -L\frac{\partial I_z}{\partial t} \tag{7.18c}$$

These equations will now be combined to form a wave equation. Differentiating Eq. (7.18a) with respect to t, Eq. (7.18b) with respect to x, and Eq. (7.18c) with

respect to z, we have

$$-\frac{\partial^2 I_z}{\partial z \partial t} - \frac{\partial^2 I_x}{\partial x \partial t} = 2C \frac{\partial^2 V_y}{\partial t^2} \tag{7.19a}$$

$$\frac{\partial^2 V_y}{\partial x^2} = -L \frac{\partial^2 I_x}{\partial t \partial x} \tag{7.19b}$$

$$\frac{\partial^2 V_y}{\partial z^2} = -L \frac{\partial^2 I_z}{\partial t \partial z} \tag{7.19c}$$

Substituting Eqs. (7.19b) and (7.19c) into Eq. (7.19a) leads to

$$\frac{\partial^2 V_y}{\partial x^2} + \frac{\partial^2 V_y}{\partial z^2} = 2LC \frac{\partial^2 V_y}{\partial t^2} \tag{7.20}$$

Equation (7.20) is the Helmholtz wave equation in two-dimensional space.

In order to show the field theory equivalence of Eqs. (7.19) and (7.20), consider Maxwell's equations

$$\nabla \times \mathbf{E} = -\mu \frac{\partial \mathbf{H}}{\partial t} \tag{7.21a}$$

and

$$\nabla \times \mathbf{H} = \epsilon \frac{\partial \mathbf{E}}{\partial t} \tag{7.21b}$$

Expansion of Eq. (7.21) in the rectangular coordinate system yields

$$\frac{\partial E_z}{\partial y} - \frac{\partial E_y}{\partial z} = -\mu \frac{\partial H_x}{\partial t} \ , \tag{7.22a}$$

$$\frac{\partial E_x}{\partial z} - \frac{\partial E_z}{\partial x} = -\mu \frac{\partial H_y}{\partial t} \ , \tag{7.22b}$$

$$\frac{\partial E_y}{\partial x} - \frac{\partial E_x}{\partial y} = -\mu \frac{\partial H_z}{\partial t} \ , \tag{7.22c}$$

$$\frac{\partial H_z}{\partial y} - \frac{\partial H_y}{\partial z} = \epsilon \frac{\partial E_x}{\partial t} \ , \tag{7.22d}$$

$$\frac{\partial H_x}{\partial z} - \frac{\partial H_z}{\partial x} = \epsilon \frac{\partial E_y}{\partial t} \ , \tag{7.22e}$$

$$\frac{\partial H_y}{\partial x} - \frac{\partial H_x}{\partial y} = \epsilon \frac{\partial E_z}{\partial t} \tag{7.22f}$$

Consider the situation for which $E_x = E_z = H_y = 0, \frac{\partial}{\partial y} = 0$. It is noticed at once that this mode is a transverse electric (TE) mode with respect to the z-axis but a transverse magnetic (TM) mode with respect to the y-axis. Thus by the principle of duality, the network in Fig. 7.9 can be used for E_y, H_x, H_z fields as well as for

E_x, E_z, H_y fields. A network capable of reproducing TE waves is also capable of reproducing TM waves. For TE waves, Eq. (7.22) reduces to

$$\frac{\partial H_x}{\partial z} - \frac{\partial H_z}{\partial x} = \epsilon \frac{\partial E_y}{\partial t} \ , \qquad (7.23a)$$

$$\frac{\partial E_y}{\partial x} = -\mu \frac{\partial H_z}{\partial t} \ , \qquad (7.23b)$$

$$\frac{\partial E_y}{\partial z} = \mu \frac{\partial H_x}{\partial t} \qquad (7.23c)$$

Taking similar steps on Eqs. (7.23a)–(7.23c) as were taken for Eqs. (7.18a)–(7.18c) results in another Helmholtz equation

$$\frac{\partial^2 E_y}{\partial x^2} + \frac{\partial^2 E_y}{\partial z^2} = \mu\epsilon \frac{\partial^2 E_y}{\partial t^2} \qquad (7.24)$$

Comparing Eqs. (7.23) and (7.24) with Eqs. 7.18 and (7.20) yields the following equivalence between the parameters

$$\boxed{\begin{aligned} E_y &\equiv V_y \\ H_x &\equiv -I_z \\ H_z &\equiv I_x \\ \mu &\equiv L \\ \epsilon &\equiv 2C \end{aligned}} \qquad (7.25)$$

Thus in the equivalent circuit:

- the voltage at shunt node is E_y,

- the current in the z direction is $-H_x$,

- the current in the x direction is H_z,

- the inductance per unit length represents the permeability of the medium,

- twice the capacitance per unit length represents the permittivity of the medium.

7.4.2 Dispersion Relation of Propagation Velocity

For the basic transmission line in the TLM which has $\mu_r = \epsilon_r = 1$, the inductance and capacitance per unit length are related by [8]

$$\frac{1}{\sqrt{(LC)}} = \frac{1}{\sqrt{(\mu_0\epsilon_0)}} = c \qquad (7.26)$$

where $c = 3 \times 10^8$ m/s is the speed of light in vacuum. Notice from Eq. (7.26) that for the equivalence made in Eq. (7.25), if voltage and current waves on each transmission line component propagate at the speed of light c, the complete network

of intersecting transmission lines represents a medium of relative permittivity twice that of free space. This implies that as long as the equivalent circuit in Fig. 7.9 is valid, the propagation velocity in the TLM mesh is $1/\sqrt{2}$ of the velocity of light. The manner in which wave propagates on the mesh is now derived.

If the ratio of the length of the transmission-line element to the free-space wavelength of the wave is $\theta/2\pi = \Delta\ell/\lambda$ (θ is called the *electrical length* of the line), the voltage and current at node i are related to those at node $i+1$ by the transfer-matrix equation (see Prob. 7.2) given as [19]

$$\begin{bmatrix} V_i \\ I_i \end{bmatrix} = \qquad\qquad (7.27)$$

$$\begin{bmatrix} (\cos\theta/2) & (j\sin\theta/2) \\ (j\sin\theta/2) & (\cos\theta/2) \end{bmatrix} \begin{bmatrix} 1 & 0 \\ (2j\tan\theta/2) & 1 \end{bmatrix} \begin{bmatrix} (\cos\theta/2) & (j\sin\theta/2) \\ (j\sin\theta/2) & (\cos\theta/2) \end{bmatrix} \begin{bmatrix} V_{i+1} \\ I_{i+1} \end{bmatrix}$$

If the waves on the periodic structure have a propagation constant $\gamma_n = \alpha_n + j\beta_n$, then

$$\begin{bmatrix} V_i \\ I_i \end{bmatrix} = \begin{bmatrix} e^{\gamma_n \Delta\ell} & 0 \\ 0 & e^{\gamma_n \Delta\ell} \end{bmatrix} \begin{bmatrix} V_{i+1} \\ I_{i+1} \end{bmatrix} \qquad (7.28)$$

Solution of Eqs. (7.27) and (7.28) gives

$$\cosh(\gamma_n \Delta\ell) = \cos(\theta) - \tan(\theta/2)\sin(\theta) \qquad (7.29)$$

This equation describes the range of frequencies over which propagation can take place (passbands), i.e.,

$$|\cos(\theta) - \tan(\theta/2)\sin(\theta)| < 1 , \qquad (7.30a)$$

and the range of frequencies over which propagation cannot occur (stop-bands), i.e.,

$$|\cos(\theta) - \tan(\theta/2)\sin(\theta)| > 1 \qquad (7.30b)$$

For the lowest frequency propagation region,

$$\gamma_n = j\beta_n \qquad (7.31a)$$

and

$$\theta = \frac{2\pi\,\Delta\ell}{\lambda} = \frac{\omega}{c}\Delta\ell \qquad (7.31b)$$

Introducing Eq. (7.31) in Eq. (7.29), we obtain

$$\cos(\beta_n \Delta\ell) = \cos\left(\frac{\omega\Delta\ell}{c}\right) - \tan\left(\frac{\omega\Delta\ell}{2c}\right)\sin\left(\frac{\omega\Delta\ell}{c}\right) \qquad (7.32)$$

Applying trigonometric identities

$$\sin(2A) = 2\sin(A)\cos(A)$$

and

$$\cos(2A) = 1 - 2\sin^2(A)$$

to Eq. (7.32) results in

$$\sin\left(\frac{\beta_n \Delta\ell}{2}\right) = \sqrt{2}\sin\left(\frac{\omega\Delta\ell}{2c}\right) \tag{7.33}$$

which is a transcendental equation. If we let r be the ratio of the velocity u_n of the waves on the network to the free-space wave velocity c, then

$$r = u_n/c = \frac{\omega}{\beta_n c} = \frac{2\pi}{\lambda\beta_n} \tag{7.34a}$$

or

$$\beta_n = \frac{2\pi}{\lambda r} \tag{7.34b}$$

Substituting Eqs. (7.34) into Eq. (7.33), the transcendental equation becomes

$$\sin\left(\frac{\pi}{r} \cdot \frac{\Delta\ell}{\lambda}\right) = \sqrt{2}\sin\left(\frac{\pi\Delta\ell}{\lambda}\right) \tag{7.35}$$

By selecting different values of $\Delta\ell/\lambda$, the corresponding values of $r = u_n/c$ can be obtained numerically as in Fig. 7.11 for two-dimensional problems. From Fig. 7.11, we conclude that the TLM can only represent Maxwell's equations over the range of frequencies from zero to the first network cutoff frequency, which occurs at $\omega\Delta\ell/c = \pi/2$ or $\Delta\ell/\lambda = 1/4$. Over this range, the velocity of the waves behaves according to the characteristic of Fig. 7.11. For frequencies much smaller than the network cutoff frequency, the propagation velocity approximates to $1/\sqrt{2}$ of the free-space velocity.

Following the same procedure, the dispersion relation for three-dimensional problems can be derived as

$$\sin\left(\frac{\pi}{r} \cdot \frac{\Delta\ell}{\lambda}\right) = 2\sin\left(\pi\frac{\Delta\ell}{\lambda}\right) \tag{7.36}$$

Thus for low frequencies ($\Delta\ell/\lambda < 0.1$), the network propagation velocity in three-dimensional space may be considered constant and equal to $c/2$.

7.4.3 Scattering Matrix

If $_kV_n^i$ and $_kV_n^r$ are the voltage impulses incident upon and reflected from terminal n of a node at time $t = k\Delta\ell/c$, we derive the relationship between the two quantities as follows. Let us assume that a voltage impulse function of unit magnitude is launched
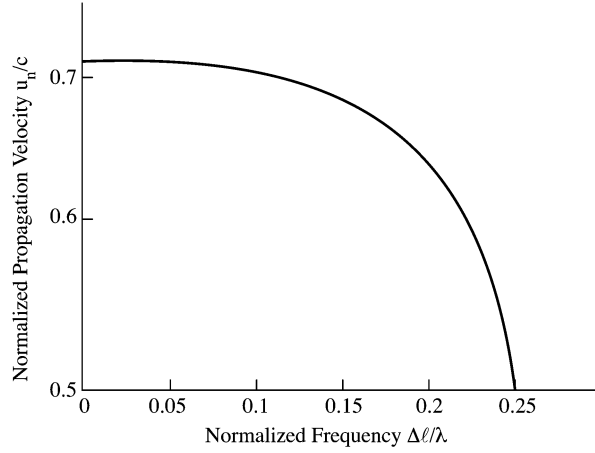
Figure 7.11
Dispersion of the velocity of waves in a two-dimensional TLM network.

into terminal 1 of a node, as shown in Fig. 7.12(a), and that the characteristic resistance of the line is normalized. A unit-magnitude delta function of voltage and current will then travel towards the junction with unit energy ($S_i = 1$). Since line 1 has three other lines joined to it, its effective terminal resistance is 1/3. With the knowledge of its reflection coefficient, both the reflected and transmitted voltage impulses can be calculated. The reflection coefficient is

$$\Gamma = \frac{R_L - R_o}{R_L + R_o} = \frac{1/3 - 1}{1/3 + 1} = -\frac{1}{2} \tag{7.37}$$

so that the reflected and transmitted energies are

$$S_r = S_i \Gamma^2 = \frac{1}{4} \tag{7.38a}$$

$$S_t = S_i \left(1 - \Gamma^2\right) = \frac{3}{4} \tag{7.38b}$$

where subscripts i, r, and t indicate incident, reflected, and transmitted quantities, respectively. Thus a voltage impulse of $-1/2$ is reflected back in terminal 1, while a voltage impulse of $1/2 = [\frac{3}{4} \div 3]^{1/2}$ will be launched into each of the other three terminals as shown in Fig. 7.12(b).

The more general case of four impulses being incident on four branches of a node can be obtained by applying the superposition principle to the previous case of a single pulse. Hence, if at time $t = k\Delta\ell/c$, voltage impulses $_kV_1^i$, $_kV_2^i$, $_kV_3^i$, and $_kV_4^i$ are incident on lines 1 to 4, respectively, at any node as in Fig. 7.12(c), the combined voltage reflected along line 1 at time $t = (k + 1)\Delta\ell/c$ will be [9, 10]

$$_{k+1}V_1^r = \frac{1}{2} \left\langle _kV_2^i + _kV_3^i + _kV_4^i - _kV_1^i \right\rangle \tag{7.39}$$
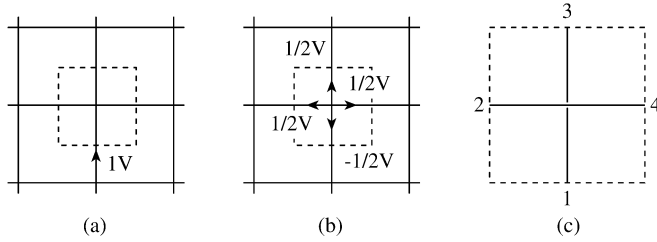
Figure 7.12
The impulse response of a node in a matrix.

In general, the total voltage impulse reflected along line n at time $t = (k + 1)\Delta\ell/c$ will be

$$_{k+1}V_n^r = \frac{1}{2}\left[\sum_{m=1}^{4} {_k}V_m^i\right] - {_k}V_n^i, \qquad n = 1, 2, 3, 4 \tag{7.40}$$

This idea is conveniently described by a *scattering matrix* equation relating the reflected voltages at time $(k + 1)\Delta\ell/c$ to the incident voltages at the previous time step $k\Delta\ell/c$:

$$\begin{bmatrix} V_1 \\ V_2 \\ V_3 \\ V_4 \end{bmatrix}_{k+1}^{r} = \frac{1}{2}\begin{bmatrix} -1 & 1 & 1 & 1 \\ 1 & -1 & 1 & 1 \\ 1 & 1 & -1 & 1 \\ 1 & 1 & 1 & -1 \end{bmatrix} \begin{bmatrix} V_1 \\ V_2 \\ V_3 \\ V_4 \end{bmatrix}_{k}^{i} \tag{7.41}$$

Also an impulse emerging from a node at position (z, x) in the mesh (reflected impulse) becomes automatically an incident impulse at the neighboring node. Hence

$$\begin{aligned}
{_{k+1}}V_1^i(z, x + \Delta\ell) &= {_{k+1}}V_3^r(z, x) \\
{_{k+1}}V_2^i(z + \Delta\ell, x) &= {_{k+1}}V_4^r(z, x) \\
{_{k+1}}V_3^i(z, x - \Delta\ell) &= {_{k+1}}V_1^r(z, x) \\
{_{k+1}}V_4^i(z - \Delta\ell, x) &= {_{k+1}}V_2^r(z, x)
\end{aligned} \tag{7.42}$$

Thus by applying Eqs. (7.41) and (7.42), the magnitudes, positions, and directions of all impulses at time $(k + 1)\Delta\ell/c$ can be obtained at each node in the network provided that their corresponding values at time $k\Delta\ell/c$ are known. The impulse response may, therefore, be found by initially fixing the magnitude, position, and direction of travel of impulse voltages at time $t = 0$, and then calculating the state of the network at successive time intervals. The scattering process forms the basic algorithm of the TLM method [10, 17].

The propagating of pulses in the TLM model is illustrated in Fig. 7.13, where the first two iterations following an initial excitation pulse in a two-dimensional shunt-
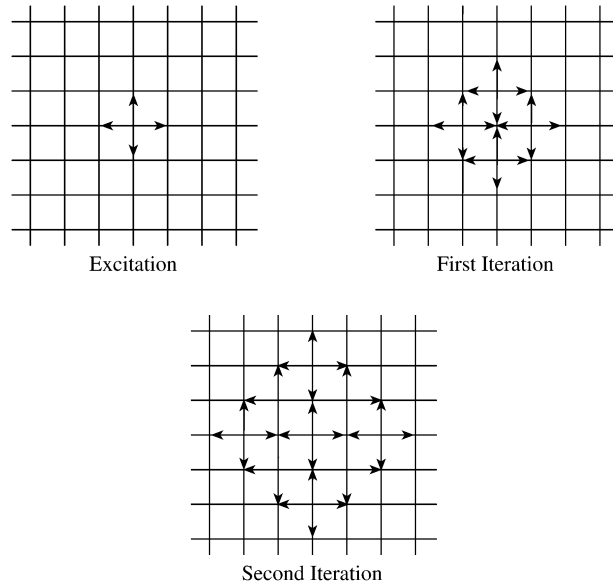
Figure 7.13
Scattering in a two-dimensional TLM network excited by a Dirac impulse.

connected TLM are shown. We have assumed free-space propagation for the sake of simplicity.

7.4.4 Boundary Representation

Boundaries are usually placed halfway between two nodes in order to ensure synchronism. In practice, this is achieved by making the mesh size $\Delta\ell$ an integer fraction of the structure's dimensions.

Any resistive load at boundary C (see Fig. 7.10) may be simulated by introducing a reflection coefficient Γ

$$_{k+1}V_4^i(p,q) = {}_kV_2^r(p+1,q) = \Gamma\left[{}_kV_4^r(p,q)\right] \tag{7.43}$$

where

$$\Gamma = \frac{R_s - 1}{R_s + 1} \tag{7.44}$$

and R_s is the surface resistance of the boundary normalized by the line characteristic impedance. If, for example, a perfectly conducting wall ($R_s = 0$) is to be simulated along boundary C, Eq. (7.44) gives $\Gamma = -1$, which represents a short circuit, and

$$_{k+1}V_4^i(p,q) = -{}_kV_4^r(p,q) \tag{7.45}$$

is used in the simulation. For waves striking the boundary at arbitrary angles of incidence, a method for modeling free-space boundaries is discussed in [20].

7.4.5 Computation of Fields and Frequency Response

We continue with the TE mode of Eq. (7.23) as our example and calculate E_y, H_x, and H_z. E_y at any point corresponds to the node voltage at the point, H_z corresponds to the net current entering the node in the x direction (see Eq. (7.25)), while H_x is the net current in the negative z direction. For any point $(z = m, x = n)$ on the grid of Fig. 7.10, we have for each kth transient time

$$_kE_y(m, n) = \frac{1}{2}\left[_kV_1^i(m, n) + _kV_2^i(m, n) + _kV_3^i(m, n) + _kV_4^i(m, n)\right] \quad (7.46)$$

$$-\ _kH_x(m, n) = _kV_2^i(m, n) - _kV_4^i(m, n) , \quad (7.47)$$

and

$$_kH_z(m, n) = _kV_3^i(m, n) - _kV_1^i(m, n) \quad (7.48)$$

Thus, a series of discrete delta-function of magnitudes E_y, H_x, and H_z corresponding to time intervals of $\Delta\ell/c$ are obtained by the iteration of Eqs. (7.41) and (7.42). (Notice that reflections at the boundaries A and B in Fig. 7.10 will cancel out, thus $H_z = 0$.) Any point in the mesh can serve as an output or observation point. Equations (7.46) to (7.48) provide the output-impulse functions for the point representing the response of the system to an impulsive excitation. These output functions may be used to obtain the output waveform. For example, the output waveform corresponding to a pulse input may be obtained by convolving the output-impulse function with the shape of the input pulse.

Sometimes we are interested in the response to a sinusoidal excitation. This is obtained by taking the Fourier transform of the impulse response. Since the response is a series of delta functions, the Fourier transform integral becomes a summation, and the real and imaginary parts of the output spectrum are given by [9, 10]

$$\text{Re}\left[F(\Delta\ell/\lambda)\right] = \sum_{k=1}^{N} {}_kI \cos\left(\frac{2\pi k \Delta\ell}{\lambda}\right) \quad (7.49a)$$

$$\text{Im}\left[F(\Delta\ell/\lambda)\right] = \sum_{k=1}^{N} {}_kI \sin\left(\frac{2\pi k \Delta\ell}{\lambda}\right) \quad (7.49b)$$

where $F(\Delta\ell/\lambda)$ is the frequency response, $_kI$ is the value of the output impulse response at time $t = k\Delta\ell/c$, and N is the total number of time intervals for which the calculation is made. Henceforth, N will be referred to as the number of iterations.

7.4.6 Output Response and Accuracy of Results

The output impulse function, in terms of voltage or current, may be taken from any point in the TLM mesh. It consists of a train of impulses of varying magnitude in the time domain separated by a time interval $\Delta\ell/c$. Thus, the frequency response obtained

by taking the Fourier transform of the output response consists of series of delta functions in the frequency domain corresponding to the discrete modal frequencies for which a solution exists. For practical reasons, the output response has to be truncated, and this results in a spreading of the solution delta function $\sin x/x$ type of curves.

To investigate the accuracy of the result, let the output response be truncated after N iterations. Let $V_{out}(t)$ be the output impulse function taken within $0 < t < N\Delta\ell/c$. We may regard $V_{out}(t)$ as an impulse function $V_\infty(t)$, taken within $0 < t < \infty$, multiplied by a unit pulse function $V_p(t)$ of width $N\Delta\ell/c$, i.e.,

$$V_{out}(t) = V_\infty(t) \times V_p(t) \tag{7.50}$$

where

$$V_p = \begin{cases} 1, & 0 \le t \le N\Delta\ell/c \\ 0, & \text{elsewhere} \end{cases} \tag{7.51}$$

Let $S_{out}(f)$, $S_\infty(f)$, and $S_p(f)$ be the Fourier transform of $V_{out}(t)$, $V_\infty(t)$, and $V_p(t)$, respectively. The Fourier transform of Eq. (7.50) is the convolution of $S_\infty(f)$ and $S_p(f)$. Hence

$$S_{out}(f) = \int_{-\infty}^{\infty} S_\infty(\alpha) S_p(f - \alpha)\, d\alpha \tag{7.52}$$

where

$$S_p(f) = \frac{N\Delta\ell}{c} \frac{\sin \dfrac{\pi N \Delta\ell f}{c}}{\dfrac{\pi N \Delta\ell f}{c}} e^{-(\pi N\Delta\ell f)/c} \tag{7.53}$$

which is of the form $\sin x/x$. Equations (7.52) and (7.53) show that $S_p(f)$ is placed in each of the positions of the exact response $S_\infty(f)$. Since the greater the number of iterations N the sharper the maximum peak of the curve, the accuracy of the result depends on N. Thus the solution of a wave equation by TLM method involves the following four steps [21]:

1. Space discretization: The solution region is divided into a number of blocks to fit the geometrical and frequency requirements. Each block is replaced by a network of transmission lines interconnected to form a "node." Transmission lines from adjacent nodes are connected to form a mesh describing the entire solution region.

2. Excitation: This involves imposing the initial conditions and source terms.

3. Scattering: With the use of the scattering matrix, pulses propagate along transmission lines toward each node. At each new time step, a multiple of propagation time δt, scattered pulses from each node become incident on adjacent nodes. The scattering and connection processes may be repeated to simulate propagation for any desired length of time.

4. Output: At any time step, voltages and currents on transmission lines are available. These represent the electric and magnetic fields corresponding to the particular problem and excitation. The quantities available at each time step are the solution in the time domain — there is no need for an iterative solution procedure. If desired, frequency-domain information may be obtained by using Fourier transform techniques.

The following examples are taken from Johns's work [9, 18].

Example 7.2

The FORTRAN program in Fig. 7.14 is for the numerical calculations of one-dimensional TEM wave problems. It should be mentioned that the computer program in this example and the following ones are modified versions of those in Agba [22]. The calculations were carried out on a 25 by 11 rectangular matrix. TEM field-continuation boundaries were fixed along $x = 2$ and $x = 10$, producing boundaries, in effect, along the lines $x = 1.5$ and $x = 10.5$. The initial impulse excitation was on all points along the line $z = 4$, and the field along this line was set to zero at all subsequent time intervals. In this way, interference from boundaries to the left of the excitation line was avoided. Calculations in the z direction were terminated at $z = 24$, so that no reflections were received from points at $z = 25$ in the matrix, and the boundary C in Fig. 7.10, situated at $z = 24.5$, was therefore matched to free space. The output-impulse response for E_y and H_x was taken at the point $z = 14$, $x = 6$, which is 10.5 mesh points away from the boundary C, for 100, 150, and 200 iterations.

Since the velocity of waves on the matrix is less than that in free space by a factor u_n/c (see Fig. 7.11), the effective intrinsic impedance presented by the network matrix is less by the same factor. The magnitude of the wave impedance on the matrix, normalized to the intrinsic impedance of free space, is given by $Z = |E_y|/|H_x|$ and is tabulated in Table 7.2, together with $\text{Arg}(Z)$, for the various numbers of iterations made. A comparison is made with the exact impedance values [14].

Table 7.2 Normalized Impedance of a TEM Wave with Free-Space Discontinuity

	TLM results						Exact results	
$\Delta\ell/\lambda$	$|Z|$	$\text{Arg}(Z)$	$|Z|$	$\text{Arg}(Z)$	$|Z|$	$\text{Arg}(Z)$	$|Z|$	$\text{Arg}(Z)$
Number of iterations	100		150		200			
0.002	0.9789	−0.1368	0.9730	−0.1396	0.9781	−0.1253	0.9747	−0.1282
0.004	0.9028	−0.2432	0.8980	−0.2322	0.9072	−0.2400	0.9077	−0.2356
0.006	0.8114	−0.3068	0.8229	−0.2979	0.8170	−0.3046	0.8185	−0.3081
0.008	0.7238	−0.3307	0.7328	−0.3457	0.7287	−0.3404	0.7256	−0.3390
0.010	0.6455	−0.3201	0.6367	−0.3350	0.6396	−0.3281	0.6414	−0.3263
0.012	0.5783	−0.2730	0.5694	−0.2619	0.5742	−0.2680	0.5731	−0.2707
0.014	0.5272	−0.1850	0.5313	−0.1712	0.5266	−0.1797	0.5255	−0.1765
0.016	0.4993	−0.0609	0.5043	−0.0657	0.5009	−0.0538	0.5018	−0.0545
0.018	0.5002	−0.0790	0.4987	−0.0748	0.5057	−0.0785	0.5057	0.0768

```
0001    C ***********************************************************
0002    C THIS PROGRAM APPLIES THE TLM METHOD TO SOLVE
0003    C ONE-DIMENSIONAL WAVE PROBLEMS. THE SPECIFIC EXAMPLE
0004    C SOLVED HERE IS DESCRIBED AS FOLLOWS:-
0005    C
0006    C THE TEM WAVES ON A 25 X 11 MATRIX
0007    C THE BOUNDARIES ARE AT X = 2 AND X = 10.
0008    C INITIAL IMPULSE EXCITATION IS ALONG Z = 4 AT t = 0
0009    C AND SUBSEQUENTLY THIS LINE IS SET TO ZERO. THE GRID
0010    C IS TERMINATED AT Z = 25. OUTPUT IS TAKEN AT Z = 14,
0011    C X = 6 FOR Ey AND Hx FOR 100,150,200 ITERATIONS
0012    C VI(IT,I,J,K) -- ARRAY FOR INCIDENT VOLTAGE
0013    C VR(IT,I,J,K) -- ARRAY FOR REFLECTED VOLTAGE
0014    C IT = 1        -- FOR PREVIOUS PULSE VALUE
0015    C    = 2        -- FOR CURRENT PULSE VALUE
0016    C I,J       -- CORRESPOND TO NODE LOCATION (Z,X)
0017    C K = 1 ..4     -- FOR TERMINALS, SEE FIG. 6C
0018    C NX            -- INDEX OF NODES IN X-DIRECTION
0019    C NZ      -- INDEX OF NODES IN Z-DIRECTION
0020    C NX/NZ B,E    -- INDEX OF BEGINNING,END NODE
0021    C NX/NZ O      -- INDEX OF OUTPUT NODE
0022    C      GAMMA        -- REFLECTION COEFFICIENT AT
0023    C                       THE BOUNDARY C
0024    C      DELTA       -- MESH SIZE DIVIDED BY LAMDA
0025    C      ITRATE      -- NO. OF ITERATIONS
0026    C***********************************************************
0027
0028          IMPLICIT  INTEGER*2(I-N),REAL*8(A,D-H,O-Y),
0029         1          COMPLEX*8(C,Z),
0030          DIMENSION VI(2,25,11,4),VR(2,25,11,4),
0031         1          OUT(20,10),EFI(20),EFR(20),
0032         2    HFI(20),HFR(20)
0033
0034          DATA NXB,NXE,NZB,NZE,NT,ITRATE/2,10,4,24,4,200/
0035          DATA NXO,NZO,PIE,GAMMA,DELTA/6,14,3.1415927,0,.002/
0036
0037    C STEP #1 ********************************************
0038    C INSERT INITIAL PULSE EXCITATION ALONG LINE Z = 4
0039    C
0040          DO 10 J = NXB, NXE
0041    10    VI(1,NZB+1,J,2) = 1.0
0042    C
0043    C STEP #2 ********************************************
0044    C USING EQS. (7.40) TO (7.42), CALCULATE THE
0045    C REFLECTED VOLTAGE AND SUBMIT IT DIRECTLY
0046    C TO THE NEIGHBORING NODE.
0047    C
0048          DO 90 ITIME = 1, ITRATE
0049             IT = 2
0050          DO 50 I  = NZB+1, NZE
0051          DO 50 J  = NXB, NXE
0052            SUM = 0.0
0053          DO 20 K = 1, NT
0054    20      SUM = SUM + VI(IT-1,I,J,K)
0055          DO 30 K = 1, NT
0056          VR(IT,I,J,K) = 0.5*SUM - VI(IT-1,I,J,K)
0057    30    CONTINUE
0058    40    CONTINUE
0059            VI(IT,I,J-1,3) = VR(IT,I,J,1)
0060            VI(IT,I-1,J,4) = VR(IT,I,J,2)
```

Figure 7.14

Computer program for Example 7.2 *(Continued).*

```
0061                    VI(IT,I,J+1,1) = VR(IT,I,J,3)
0062                    VI(IT,I+1,J,2) = VR(IT,I,J,4)
0063    C
0064    C STEP #3 ********************************************
0065    C USING EQS. (7.43) AND (7.44), INSERT BOUNDARY CONDITIONS
0066    C
0067             IF(J .EQ. NXE)VI(IT,I,NXE,3)=VR(IT,I,NXE,1)
0068             IF(J .EQ. NXB)VI(IT,I,NXB,1)=VR(IT,I,NXB,3)
0069             IF(I .EQ. NZE)VI(IT,NZE,J,4)=GAMMA*VR(IT,NZE,J,4)
0070
0071    50       CONTINUE
0072    C
0073    C STEP #4 ********************************************
0074    C USING EQS. (7.46) - (7.49), CALCULATE IMPULSE RESPONSE
0075    C OF Ey and Hx AT Z=NZO,X=NXO
0076    C
0077             EI = 0.0
0078             DO 60 K = 1, NT
0079    60       EI = EI + VI(IT,NZO,NXO,K) * 0.5
0080             HI = VI(IT,NZO,NXO,2) - VI(IT,NZO,NXO,4)
0081    C
0082    C SUM THE FREQUENCY RESPONSE (imaginary and real
0083    C parts) FOR DIFFERENT VALUES OF MESH-SIZE DIVIDED
0084    C BY WAVELENGTH
0085    C
0086                 DEL = DELTA
0087                 II = 1
0088             DO 70 K = 1, 20
0089               T = DFLOAT(ITIME)
0090               EFI(K) = EFI(K) + EI * SIN(2 * PIE * T * DEL)
0091               EFR(K) = EFR(K) + EI * COS(2 * PIE * T * DEL)
0092               HFI(K) = HFI(K) + HI * SIN(2 * PIE * T * DEL)
0093               HFR(K) = HFR(K) + HI * COS(2 * PIE * T * DEL)
0094               OUT(K,II) = DEL
0095    70         DEL = DEL + 0.002
0096    C
0097    C SAVE THE CURRENT PULSE MAGNITUDE FOR NEXT ITERATION
0098    C
0099             DO 80 I = NZB, NZE
0100             DO 80 J = NXB, NXE
0101             DO 80 K = 1, NT
0102             VI(IT-1,I,J,K) = VI(IT,I,J,K)
0103             VR(IT-1,I,J,K) = VR(IT,I,J,K)
0104    80       CONTINUE
0105             IT = ITIME
0106                 IF((IT .EQ. 100) .OR.( IT .EQ. 150)
0107    1                         .OR.(IT .EQ. 200))THEN
0108               PRINT*, IT
0109               IF(IT .EQ. 100) II = 2
0110               IF(IT .EQ. 150) II = 3
0111               IF(IT .EQ. 200) II = 4
0112    C
0113    C STEP #5 ********************************************
0114    C CALCULATE MAGNITUDE & ARGUMENT OF IMPEDANCE
0115    C
0116                 DO K = 1, 20
0117                 CEF = CMPLX(EFR(K),EFI(K))
0118                 CHF = CMPLX(HFR(K),HFI(K))
0119                 OUT(K,II) = CABS(CEF)/CABS(CHF) ! MAGNITUDE
```

Figure 7.14

(Cont.) **Computer program for Example 7.2 *(Continued).***

```
0120
0121              ZARG = CEF/CHF
0122              XZ   = REAL( ZARG )
0123              YZ   = AIMAG( ZARG )
0124              XYZ  = YZ / XZ
0125              OUT(K,II+4) = -ATAN( XYZ ) ! ARGUMENT
0126
0127              END DO
0128              END IF
0129     90       CONTINUE
0130     C
0131     C STEP #6 ******************************************
0132     C CALCULATE EXACT VALUE OF IMPEDANCE [ REF. 13]
0133     C
0134              DEL = DELTA
0135              DO 100 K = 1, 20
0136              R2 = 1.0/TRANSC(DEL)
0137              PRINT*,R2
0138              R3 = TAN(21.0*R2*PIE*DEL)
0139              CNUM = CMPLX(R2, R3)
0140              RIG = R2 * R3
0141              RR = 1.0
0142              CDEN = CMPLX(RR, RIG)
0143              OUT(K,5) = CABS(CNUM)/(CABS(CDEN)*R2)
0144              ZARG = CNUM/CDEN
0145              XZ   = REAL( ZARG )
0146              YZ   = AIMAG( ZARG )
0147              XYZ  = YZ / XZ
0148              OUT(K,9) = ATAN( XYZ )
0149              DEL = DEL + .002
0150    100       CONTINUE
0151              DO 110 K = 1, 20
0152    110       WRITE(6,120) (OUT(K,J),J = 1, 10)
0153    120       FORMAT(2X,10F10.4)
0154              STOP
0155              END

0001     C ******************************************
0002     C THIS SUBPROGRAM USE EQ. (7.35) TO CALCULATE
0003     C RATIO Vn/c, GIVEN (DELTA/LAMDA).
0004     C
0005              FUNCTION TRANSC(DELTA)
0006              REAL LAMDA,LAMDAC
0007              PIE = 3.14159265
0008              TETA = PIE * DELTA
0009              TET  = SQRT(2.0) * SIN(TETA)
0010              TRANSC = TETA/ASIN(TET)
0011              RETURN
0012              END
```

Figure 7.14

(Cont.) **Computer program for Example 7.2.**

Example 7.3

The second example is on a rectangular waveguide with a simple load. The FOR-
TRAN program used for the numerical analysis is basically similar to that of one-
dimensional simulation. A 25×11 matrix was used for the numerical analysis of
the waveguide. Short-circuit boundaries were placed at $x = 2$ and $x = 10$, the
width between the waveguide walls thus being 9 mesh points. The system was ex-
cited at all points along the line $z = 2$, and the impulse function of the output was
taken from the point $(x = 6, z = 12)$. The C boundary at $z = 24$ represented an

abrupt change to the intrinsic impedance of free space. The minor changes in the program of Fig. 7.14 are shown in Fig. 7.15. The cutoff frequency for the waveguide occurs [19] at $\Delta\ell/\lambda_n = 1/18$, λ_n is the network-matrix wavelength, which corresponds to $\Delta\ell/\lambda = \sqrt{2}/18$ since

$$\frac{\lambda_n}{\lambda} = \frac{u_n}{c} = \frac{\sqrt{\mu_o\epsilon_o}}{\sqrt{\mu_n\epsilon_n}} = \frac{\sqrt{LC}}{\sqrt{2LC}} = \frac{1}{\sqrt{2}}$$

A comparison between the results for the normalized guide impedance using this method is made with exact results in Table 7.3. ▯

Table 7.3 Normalized Impedance of a Rectangular Waveguide with Simple Load

$\Delta\ell/\lambda$	TLM results		Exact results	
	$\|Z\|$	$\text{Arg}(Z)$	$\|Z\|$	$\text{Arg}(Z)$
0.020	1.9391	0.8936	1.9325	0.9131
0.021	2.0594	0.6175	2.0964	0.6415
0.022	1.9697	0.3553	2.0250	0.3603
0.023	1.7556	0.1530	1.7800	0.1438
0.024	1.5173	0.0189	1.5132	0.0163
0.025	1.3036	-0.0518	1.2989	-0.0388
0.026	1.1370	-0.0648	1.1471	-0.0457
0.027	1.0297	-0.0350	1.0482	-0.0249
0.028	0.9776	0.0088	0.9900	0.0075
0.029	0.9620	0.0416	0.9622	0.0396
0.030	0.9623	0.0554	0.9556	0.0632

7.5   Inhomogeneous and Lossy Media in TLM

In our discussion on the transmission-line-matrix (TLM) method in the last section, it was assumed that the medium in which wave propagates was homogeneous and lossless. In this section, we consider media that are inhomogeneous or lossy or both. This necessitates that we modify the equivalent network of Fig. 7.9 and the corresponding transmission line matrix of Fig. 7.10. Also, we need to draw the corresponding equivalence between the network and Maxwell's equations and derive the scattering matrix. We will finally consider how lossy boundaries are represented.

```
           :
           :
           :
0034            DATA NXB,NXE,NZB,NZE,NT,ITRATE/2,10,2,24,4,200/
0035            DATA NXO,NZO,PIE,GAMMA,DELTA/6,12,3.1415927,0,.02/

           :
           :
           :

0064    C STEP #3 *****************************************
0065    C USING EQS. (7.43) AND (7.44), INSERT BOUNDARY CONDITIONS
0066    C
0067            IF(J .EQ. NXE)VI(IT,I,NXE,3)= - VR(IT,I,NXE,1)
0068            IF(J .EQ. NXB)VI(IT,I,NXB,1)=VR(IT,I,NXB,1)
0069            IF(I .EQ. NZE)VI(IT,NZE,J,4)=GAMMA*VR(IT,NZE,J,4)

           :
           :
           :


0095    70      DEL = DEL + 0.001

           :
           :
           :
```

Figure 7.15

Modification in the program in Fig. 7.14 for simulating waveguide problem in Example 7.3.

7.5.1 General Two-Dimensional Shunt Node

To account for the inhomogeneity of a medium (where ϵ is not constant), we introduce additional capacitance at nodes to represent an increase in permittivity [17], [23]–[25]. We achieve this by introducing an additional length of line or stub to the node as shown in Fig. 7.16 (a). The stub of length $\Delta \ell/2$ is open circuited at the end and is of variable characteristic admittance Y_o relative to the unity characteristic admittance assumed for the main transmission line. At low frequencies, the effect of the stub is to add to each node an additional lumped shunt capacitance $CY_o\Delta\ell/2$, where C is the shunt capacitance per unit length of the main lines that are of unity characteristic admittance. Thus at each node, the total shunt capacitance becomes

$$C' = 2C\Delta\ell + CY_o\Delta\ell/2$$

or

$$C' = 2C\Delta\ell\,(1 + Y_o/4) \tag{7.54}$$

To account for the loss in the medium, we introduce a power-absorbing line at each node, lumped into a single resistor, and this is simulated by an infinite or matched line of characteristic admittance G_o normalized to the characteristic impedance of the main lines as illustrated in Fig. 7.16 (b).

Due to these additional lines, the equivalent network now becomes that shown in Fig. 7.17. (Compare Fig. 7.17 with Fig. 7.9). Applying Kirchhoff's current law to
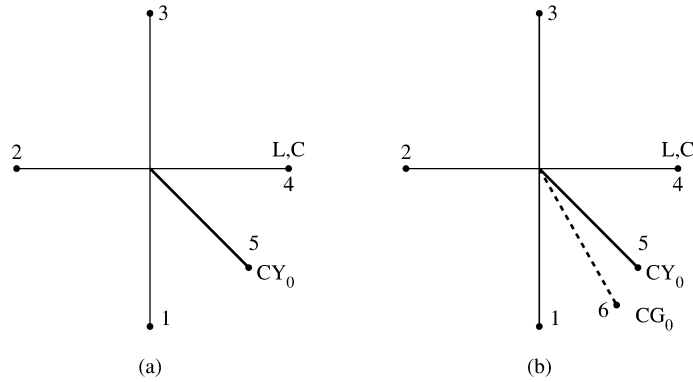
Figure 7.16

**A two-dimensional node with: (a) Permittivity stub, (b) permittivity and loss stub.**
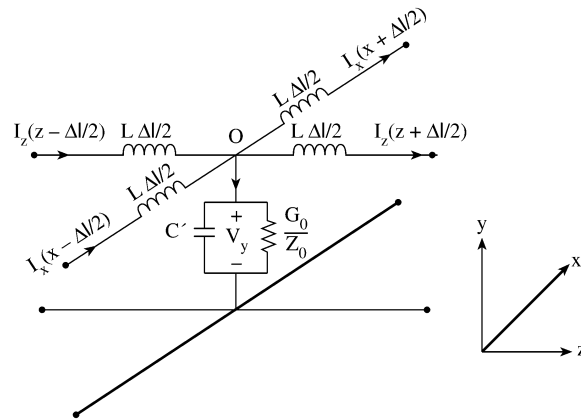
Figure 7.17

General two-dimensional shunt node.

shunt node O in the x-z plane in Fig. 7.17 and taking limits as $\Delta\ell \rightarrow 0$ results in

$$-\frac{\partial I_z}{\partial z} - \frac{\partial I_x}{\partial x} = \frac{G_o V_y}{Z_o \Delta\ell} + 2C\left(1 + Y_o/4\right)\frac{\partial V_y}{\partial t} \tag{7.55}$$

Expanding Maxwell's equations $\nabla \times \mathbf{E} = -\mu\dfrac{\partial \mathbf{H}}{\partial t}$ and $\nabla \times \mathbf{H} = \sigma\mathbf{E} + \epsilon\dfrac{\partial \mathbf{E}}{\partial t}$ for $\partial/\partial y \equiv 0$ leads to

$$\frac{\partial H_x}{\partial z} - \frac{\partial H_z}{\partial x} = \sigma E_y + \epsilon_o\epsilon_r\frac{\partial E_y}{\partial t} \tag{7.56}$$

This may be considered as denoting TE_{m0} modes with field components H_z, H_x, and E_y. From Eqs. (7.55) and (7.56), the following equivalence between the TLM

equations and Maxwell's equations can be drawn:

$$\boxed{\begin{aligned}
E_y &\equiv V_y \\
H_x &\equiv -I_z \\
H_z &\equiv I_x \\
\epsilon_o &\equiv 2C \\
\epsilon_r &\equiv \frac{4+Y_o}{4} \\
\sigma &\equiv \frac{G_o}{Z_o \Delta \ell}
\end{aligned}}
\tag{7.57}$$

where $Z_o = \sqrt{L/C}$. From Eq. (7.57), the normalized characteristic admittance G_o of the loss stub is related to the conductivity of the medium by

$$G_o = \sigma \Delta \ell Z_o \tag{7.58}$$

Thus losses on the matrix can be varied by altering the value of G_o. Also from Eq. (7.57), the variable characteristic admittance Y_o of the permittivity stub is related to the relative permittivity of the medium as

$$Y_o = 4(\epsilon_r - 1) \tag{7.59}$$

7.5.2 Scattering Matrix

We now derive the impulse response of the network comprising of the interconnection of many generalized nodes such as that in Fig. 7.17. As in the previous section, if $_k V_n(z, x)$ is unit voltage impulse reflected from the node at (z, x) into the nth coordinate direction ($n = 1, 2, \ldots, 5$) at time $k\Delta \ell/c$, then at node (z, x),

$$\boxed{
{}_{k+1}\begin{bmatrix} V_1(z, x) \\ V_2(z, x) \\ V_3(z, x) \\ V_4(z, x) \\ V_5(z, x) \end{bmatrix}^r
= [S] \;
{}_{k}\begin{bmatrix} V_3(z, x - \Delta \ell) \\ V_4(z - \Delta \ell, x) \\ V_1(z, x + \Delta \ell) \\ V_2(z + \Delta \ell, x) \\ V_5(z, x + \Delta \ell) \end{bmatrix}^i
}
\tag{7.60}$$

where $[S]$ is the scattering matrix given by

$$\boxed{
[S] = \frac{2}{Y}
\begin{bmatrix}
1 & 1 & 1 & 1 & Y_o \\
1 & 1 & 1 & 1 & Y_o \\
1 & 1 & 1 & 1 & Y_o \\
1 & 1 & 1 & 1 & Y_o \\
1 & 1 & 1 & 1 & Y_o
\end{bmatrix} - [I]
}
\tag{7.61}$$

$[I]$ is a unit matrix and $Y = 4 + Y_o + G_o$. The coordinate directions 1, 2, 3, and 4 correspond to $-x, -z, +x$, and $+z$, respectively (as in the last section), and 5 refers to the permittivity stub. Notice that the voltage V_6 (see Fig. 7.16) scattered into the

loss stub is dropped across G_o and not returned to the matrix. We apply Eq. (7.60) just as Eq. (7.41).

As in the last section, the output impulse function at a particular node in the mesh can be obtained by recording the amplitude and the time of the stream of pulses as they pass through the node. By taking the Fourier transform of the output impulse function using Eq. (7.49), the required information can be extracted.

The dispersion relation can be derived in the same manner as in the last section. If $\gamma_n = \alpha_n + j\beta_n$ is the network propagation constant and $\gamma = \alpha + j\beta$ is the propagation constant of the medium, the two propagation constants are related as

$$\frac{\beta}{\beta_n} = \frac{\theta/2}{\sin^{-1}\left[\sqrt{2(1 + Y_o/4)}\sin\theta/2\right]} \tag{7.62a}$$

$$\frac{\alpha}{\alpha_n} = \frac{\sqrt{1 - 2(1 + Y_o/4)\sin^2\theta/2}}{\sqrt{2(1 + Y_o/4)}\cos\theta/2} \tag{7.62b}$$

where $\theta = 2\pi\Delta\ell/\lambda$ and

$$\alpha = \frac{G_o}{8\Delta\ell(1 + Y_o/4)} \tag{7.63}$$

In arriving at Eq. (7.62), we have assumed that $\alpha_n\Delta\ell \ll 1$. For low frequencies, the attenuation constant α_n and phase constant β_n of the network are fairly constant so that Eq. (7.62) reduces to

$$\gamma_n = \sqrt{2(1 + Y_o/4)}\gamma \tag{7.64}$$

From this, the network velocity $u_n(= \omega/\beta_n = \beta c/\beta_n)$ of waves on the matrix is readily obtained as

$$u_n^2 = \frac{c^2}{2(1 + Y_o/4)} \tag{7.65}$$

where c is the free-space velocity of waves.

7.5.3 Representation of Lossy Boundaries

The above analysis has incorporated conductivity σ of the medium in the TLM formulation. To account for a lossy boundary [25]–[27], we define the reflection coefficient

$$\Gamma = \frac{Z_s - Z_o}{Z_s + Z_o} \tag{7.66}$$

where $Z_o = \sqrt{\mu_o/\epsilon_o}$ is the characteristic impedance of the main lines and Z_s is the surface impedance of the lossy boundary given by

$$Z_s = \sqrt{\frac{\mu\omega}{2\sigma_c}}(1 + j) \tag{7.67}$$

where μ and σ_c are the permeability and conductivity of the boundary. It is evident from Eqs. (7.66) and (7.67) that the reflection coefficient Γ is in general complex. However, complex Γ implies that the shape of the pulse functions is altered on reflection at the conducting boundary, and this cannot be accounted for in the TLM method [22]. Therefore, assuming that Z_s is small compared with Z_o and that the imaginary part of Γ is negligible,

$$\Gamma \simeq -1 + \sqrt{\frac{2\epsilon_o \omega}{\sigma_c}} \qquad (7.68)$$

where $\mu = \mu_o$ is assumed. We notice that Γ is slightly less than -1. Also, we notice that Γ depends on the frequency ω and hence calculations involving lossy boundaries are only accurate for the specific frequency; calculations must be repeated for a different value of $\Delta\ell/\lambda$. The following example is taken from Akhtarzad and Johns [24].

Example 7.4
Consider the lossy homogeneous filled waveguide shown in Fig. 7.18. The guide is 6 cm wide and 13 cm long. It is filled with a dielectric of relative permittivity $\epsilon_r = 4.9$ and conductivity $\sigma = 0.05$ mhos/m and terminated in an open circuit discontinuity. Calculate the normalized wave impedance. ⬛
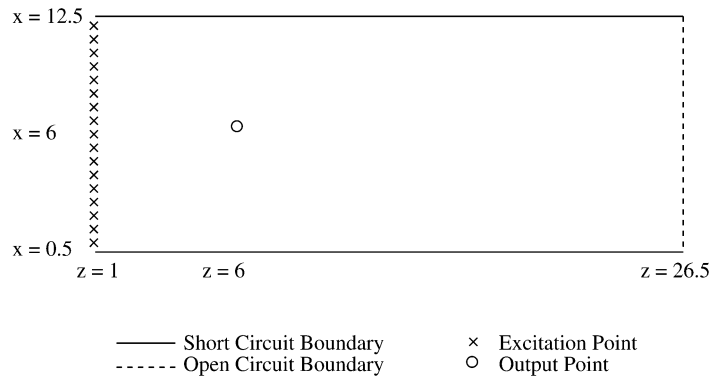

Figure 7.18
A lossy homogeneously filled waveguide.

Solution
The computer program for this problem is in Fig. 7.19. It is an extension of the program in Fig. 7.14 with the incorporation of new concepts developed in this section. Enough comments are added to make it self-explanatory. The program is suitable for a two-dimensional TE$_{m0}$ mode.

The waveguide geometry shown in Fig. 7.18 is simulated on a matrix of 12×26 nodes. The matrix is excited at all points along line $z = 1$ with impulses corresponding to E_y. The impulse function of the output at point $(z, x) = (6, 6)$ is taken after 700 iterations. Table 7.4 presents both the TLM and theoretical values of the normalized wave impedance and shows a good agreement between the two. ∎

Table 7.4 Impedance of a Homogeneously
Filled Waveguide with Losses

	TLM results		Exact results	
$\Delta\ell/\lambda$	$|Z|$	$\mathrm{Arg}(Z)$	$|Z|$	$\mathrm{Arg}(Z)$
0.003	0.0725	1.5591	0.0729	1.5575
0.006	0.1511	1.5446	0.1518	1.5420
0.009	0.2446	1.5243	0.2453	1.5205
0.012	0.3706	1.4890	0.3712	1.4840
0.015	0.5803	1.4032	0.5792	1.3977
0.018	1.0000	1.0056	0.9979	1.0065
0.021	1.1735	0.5156	1.1676	0.5121
0.024	0.5032	-0.1901	0.5093	-0.2141
0.027	0.6766	0.6917	0.6609	0.6853
0.030	0.8921	-0.3869	0.8921	-0.4185

7.6 Three-Dimensional TLM Mesh

The TLM mesh considered in Sections 7.4 and 7.5 is two-dimensional. The choice of shunt-connected nodes to represent the two-dimensional wave propagation was quite arbitrary; the TLM mesh could have equally been made up of series-connected nodes. To represent a three-dimensional space, however, we must apply a hybrid TLM mesh consisting of three shunt and three series nodes to simultaneously describe all the six field components. First of all, we need to understand what a series-connected node is.

7.6.1 Series Nodes

Figure 7.20 portrays a lossless series-connected node that is equipped with a short-circuited stub called the permeability stub. The corresponding network representation is illustrated in Fig. 7.21. The input impedance of the short-circuited stub is

$$Z_{in} = jZ_o\sqrt{\frac{L}{C}} \tan\left(\frac{\omega\Delta\ell}{2c}\right) \simeq j\omega L Z_o \Delta\ell/2 \qquad (7.69)$$

```
0001        C===========================================================
0002        C THIS PROGRAM SOLVES A TYPICAL TWO-DIMENSIONAL
0003        C WAVE PROPAGATION PROBLEM AS STATED BELOW:
0004        C A WAVE GUIDE 6cm X 13cm LONG IS FILLED WITH A
0005        C DIELECTRIC OF RELATIVE PERMITTIVITY EQUAL TO 4.9
0006        C AND CONDUCTIVITY 0.05 MHO/M. THIS GEOMETRY IS
0007        C BEING SIMULATED ON A MATRIX OF 12 X 26 NODES.
0008        C THE MATRIX WAS EXCITED AT ALL POINTS ALONG THE
0009        C LINE Z = 1 WITH IMPULSES CORRESPONDING TO Ey.
0010        C THE IMPULSE FUNCTION OF THE OUTPUT WAS TAKEN FROM
0011        C THE POINT (Z = 6, X = 6) AFTER 750 ITERATIONS.
0012        C THE BOUNDARIES WERE SHORT CIRCUITED AT X = 0.5
0013        C AND X = 12.5 AND TERMINATED AT Z = 26.5 IN AN
0014        C OPEN CIRCUIT DISCONTINUITY.
0015        C VI -- ARRAY FOR INCIDENT VOLTAGE
0016        C VR -- ARRAY FOR REFLECTED VOLTAGE
0017        C NX -- INDEX OF NODES IN X-DIRECTION
0018        C NZ -- INDEX OF NODES IN Z-DIRECTION
0019        C RO -- REFLECTION COEFFIENT
0020        C DELTA  -- MESH SIZE (SPACING)
0021        C DELTA    -- MESH SIZE DIVIDED BY LAMBDA
0022
0023               IMPLICIT REAL*8(A,D-H,O-Y),COMPLEX*8(C,Z)
0024               DIMENSION VI(0:1,27,13,5),VR(0:1,27,13,5)
0025           1   ,EFI(50),EFR(50),HFI(50),HFR(50),OUT(10,5)
0026
0027               DATA NXB,NXE,NZB,NZE,NT,ITRATE/1,12,1,26,5,750/
0028               DATA NXI,NZI,NXO,NZO,RoS,RoC/0,1,6,6,-1.0,1.0/
0029               DATA Eo,Er,SIGMA,DELTA,PI/8.854E-12,4.9,0.05,
0030           1                   0.005,3.1415927/
0031
0032               Yo = 4.0 * (Er/2.0 - 1)
0033               Ur = 1.0
0034               Uo = 4.0 * PI * 1.0E-07
0035               Go = SIGMA * DELTA * SQRT( Uo/Eo )
0036               Y = 4.0 + Yo + Go
0037        C
0038        C SINCE REFLECTION COEFFICIENT, RO, DEPENDS ON
0039        C FREQUENCY, THE ITERATIONS MUST BE REPEATED FOR
0040        C EACH VALUE OF THE MESH-SIZE DIVIDED BY WAVELENGTH.
0041        C
0042               DELTA = 0.0
0043               DO 90 L = 1, 10
0044               DELTA = DELTA + 0.003
0045        C
0046        C INITIALIZE ALL NODES (BOTH FREE AND FIXED)
0047        C
0048               DO 10 I = NZB, NZE
0049               DO 10 J = NXB, NXE
0050               DO 10 K = 1, NT
0051               VI(0,I,J,K) = 0.0
0052        10     VR(0,I,J,K) = 0.0
0053        C
0054        C START THE ITERATION
0055        C
0056               DO 90 ITime = 0, ITRATE
0057               IT = 1
0058               DO 60 I  = NZB, NZE
0059               DO 50 J  = NXB, NXE
0060               SUM = 0.0
```

Figure 7.19

Computer program for Example 7.4 *(Continued).*

2001 by CRC PRESS LLC

```
0061
0062            DO 30 K = 1, 4
0063     30     SUM = SUM + VI(IT-1,I,J,K)
0064            SUM = (SUM + Yo*VI(IT-1,I,J,5)) * 2.0/Y
0065     C
0066     C  INSERT THE INITIAL CONDITION AT I = 1
0067     C
0068            IF(ITIME .EQ. O .AND. I .EQ. NZI) SUM = 1.0
0069
0070            DO 40 K = 1, NT
0071     40         VR(IT,I,J,K) = SUM - VI(IT-1,I,J,K)
0072
0073            IF(J .NE. NXB) VI(IT,I,J-1,3) = VR(IT,I,J,1)
0074            IF(I .NE. NZB+1)VI(IT,I-1,J,4)= VR(IT,I,J,2)
0075            IF(J .NE. NXE) VI(IT,I,J+1,1) = VR(IT,I,J,3)
0076            IF(I .NE. NZE) VI(IT,I+1,J,2) = VR(IT,I,J,4)
0077                VI(IT,I,J,5)   = VR(IT,I,J,5)
0078     C
0079     C INSERT THE BOUNDARY CONDITIONS
0080     C FOR THE SHORT CIRCUIT AT X = 0.5
0081     C
0082            IF(J .EQ. NXB) VI(IT,I,1,1) =RoS*VR(IT,I,1,1)
0083     C
0084     C FOR THE SHORT CIRCUIT AT X = 12.5
0085     C
0086            IF(J .EQ. NXE) VI(IT,I,J,3) =RoS*VR(IT,I,J,3)
0087     C
0088     C FOR THE OPEN CIRCUIT DISCONTINUITY AT Z = 26.5
0089     C
0090            IF(I .EQ. NZE) VI(IT,I,J,4) =RoC*VR(IT,I,J,4)
0091
0092     50     CONTINUE
0093     60     CONTINUE
0094     C
0095     C IN ORDER TO CONSERVE SPACE, THE ARRAYS
0096     C HAVE TO BE UPDATED
0097     C
0098            DO 70 I = 1, NZE
0099            DO 70 J = 1, NXE
0100            DO 70 K = 1, NT
0101            VI(IT-1,I,J,K) = VI(IT,I,J,K)
0102     70     VR(IT-1,I,J,K) = VR(IT,I,J,K)
0103     C
0104     C CALCULATE IMPULSE RESPONSE  AT Z=NZO, X=NXO
0105     C
0106            EI = 0.0
0107            DO 80 K = 1, 4
0108     80     EI = EI + VI(IT,NZO,NXO,K)
0109            EI = (EI + Yo * VI(IT,NZO,NXO,5)) * 2.0/Y
0110            HI = -(VI(IT,NZO,NXO,2)-VI(IT,NZO,NXO,4))
0111     C
0112     C SUM THE FREQUENCY RESPONSE (imaginary and
0113     C real parts) FOR DIFFERENT VALUES OF
0114     C MESH-SIZE DIVIDED BY WAVELENGTH
0115     C
0116            T = DFLOAT(ITIME)
0117            EFI(L)=EFI(L)+EI*DSIN(2.0 * PI * T * DELTA)
0118            EFR(L)=EFR(L)+EI*DCOS(2.0 * PI * T * DELTA)
0119            HFI(L)=HFI(L)+HI*DSIN(2.0 * PI * T * DELTA)
0120            HFR(L)=HFR(L)+HI*DCOS(2.0 * PI * T * DELTA)
```

Figure 7.19

(Cont.) **Computer program for Example 7.4** *(Continued).*

```
0121              OUT(L,1) = DELTA
0122              IF( ITIME .EQ. ITRATE ) THEN
0123              CEF = CMPLX(EFR(L),EFI(L))
0124              CHF = CMPLX( HFR(L), HFI(L))
0125              OUT(L,2) = CABS(CEF)/CABS(CHF)
0126      C
0127      C CALCULATE ARGUMENT Z
0128      C
0129              ZARG = CEF/CHF
0130              XZ   = REAL( ZARG )
0131              YZ   = AIMAG( ZARG )
0132              XYZ  = YZ / XZ
0133              OUT(L,3) = -ATAN( XYZ )
0134              print*,out(1,1),out(1,2),out(1,3)
0135              END IF
0136   90         CONTINUE
0137              DO 100 K = 1, L-1
0138   100        WRITE(6,110) (OUT(K,J),J = 1, 3)
0139   110        FORMAT(2X,10F10.4)
0140              STOP
0141              END
```

Figure 7.19

*(Cont.)* **Computer program for Example 7.4.**
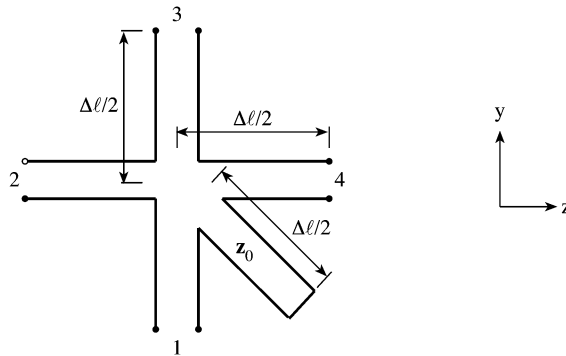
Figure 7.20

A lossless series connected node with permeability stub.

where Eq. (7.26) has been applied. This represents an impedance with inductance

$$L' = L\frac{\Delta\ell}{2}Z_o \tag{7.70}$$

Hence the total inductance on the side in which the stub is inserted is $L\Delta\ell(1 + Z_o)/2$ as in Fig. 7.21. We now apply Kirchhoff's voltage law around the series node of Fig. 7.21 and obtain

$$V_z + L\frac{\Delta\ell}{2}(1 + Z_o)\frac{\partial I_x}{\partial t} + V_y + \frac{\partial V_y}{\partial z}\Delta\ell - \left(V_z + \frac{\partial V_z}{\partial y}\Delta\ell\right) + 3L\frac{\Delta\ell}{2}\frac{\partial I_x}{\partial t} - V_y = 0$$
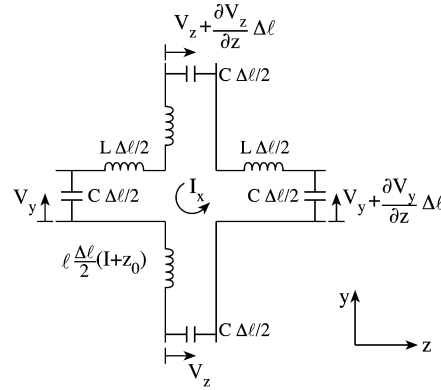
Figure 7.21
Network representation of a series node.

Dividing through by $\Delta\ell$ and rearranging terms leads to

$$\frac{\partial V_z}{\partial y} - \frac{\partial V_y}{\partial z} = 2L\left(1 + Z_o/4\right)\frac{\partial I_x}{\partial t} \qquad (7.71)$$

Note that the series node is oriented in the y-z plane. Equations for series nodes in the x-y and x-z planes can be obtained in a similar manner as

$$\frac{\partial V_y}{\partial x} - \frac{\partial V_x}{\partial y} = 2L\left(1 + Z_o/4\right)\frac{\partial I_z}{\partial t} \qquad (7.72)$$

and

$$\frac{\partial V_x}{\partial z} - \frac{\partial V_z}{\partial x} = 2L\left(1 + Z_o/4\right)\frac{\partial I_y}{\partial t} \ , \qquad (7.73)$$

respectively.

Comparing Eqs. (7.71) to (7.73) with Maxwell's equations in Eq. (7.22), the following equivalences can be identified:

$$\boxed{\begin{aligned} E_x &\equiv V_x \\ E_z &\equiv V_z \\ \mu_o &\equiv 2L \\ \mu_r &\equiv \frac{4 + Z_o}{4} \end{aligned}} \qquad (7.74)$$

A series-connected two-dimensional TLM mesh is shown in Fig. 7.22 (a). while the equivalent one-dimensional mesh is in Fig. 7.22 (b). A voltage impulse incident on a series node is scattered in accordance with Eq. (7.60), where the scattering matrix
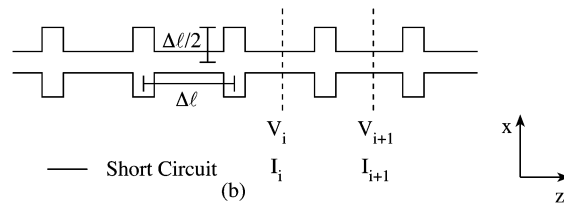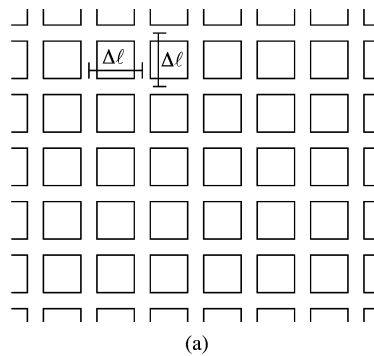
Figure 7.22
(a) A two-dimensional series-connected TLM mesh. (b) A one-dimensional series-connected TLM mesh.

is now

$$[S] = \frac{2}{Z} \begin{bmatrix} -1 & 1 & 1 & -1 & -1 \\ 1 & -1 & -1 & 1 & 1 \\ 1 & -1 & -1 & 1 & 1 \\ -1 & 1 & 1 & -1 & -1 \\ -Z_o & Z_o & Z_o & -Z_o & -Z_o \end{bmatrix} + [I] \tag{7.75}$$

$Z = 4 + Z_o$, and $[I]$ is the unit matrix. The velocity characteristic for the two-dimensional series matrix is the same as for the shunt node [24]. For low frequencies ($\Delta \ell / \lambda < 0.1$) the velocity of the waves on the matrix is approximately $1/\sqrt{2}$ of the free-space velocity. This is due to the fact that the stubs have twice the inductance per unit length, while the capacitance per unit length remains unchanged. This is the dual of the two-dimensional shunt case in which the capacitance was doubled and the inductance was unchanged.

7.6.2 Three-Dimensional Node

A three-dimensional TLM node [27] consists of three shunt nodes in conjunction with three series nodes. The voltages at the three shunt nodes represent the three components of the **E** field, while the currents of the series nodes represent the three

components of the **H** field. In the x-z plane, for example, the voltage-current equations for the shunt node are

$$\frac{\partial I_x}{\partial z} - \frac{\partial I_z}{\partial x} = 2C\frac{\partial V_y}{\partial t} \tag{7.76a}$$

$$\frac{\partial V_y}{\partial x} = -L\frac{\partial I_x}{\partial t} \tag{7.76b}$$

$$\frac{\partial V_y}{\partial z} = -L\frac{\partial I_z}{\partial t} \tag{7.76c}$$

and for the series node in the x-z plane, the equations are

$$\frac{\partial V_x}{\partial z} - \frac{\partial V_z}{\partial x} = 2L\frac{\partial I_y}{\partial t} \tag{7.77a}$$

$$\frac{\partial I_y}{\partial x} = -C\frac{\partial V_z}{\partial t} \tag{7.77b}$$

$$\frac{\partial I_y}{\partial z} = -C\frac{\partial V_x}{\partial t} \tag{7.77c}$$

Maxwell's equations $\nabla \times \mathbf{E} = \dfrac{\partial \mathbf{B}}{\partial t}$ and $\nabla \times \mathbf{H} = \epsilon\dfrac{\partial \mathbf{E}}{\partial t}$ for $\dfrac{\partial}{\partial y} \equiv 0$ give

$$\frac{\partial H_x}{\partial z} - \frac{\partial H_z}{\partial x} = \epsilon\frac{\partial E_y}{\partial t} \tag{7.78a}$$

$$\frac{\partial E_y}{\partial x} = \mu\frac{\partial H_x}{\partial t} \tag{7.78b}$$

$$\frac{\partial E_y}{\partial z} = -\mu\frac{\partial H_z}{\partial t} \tag{7.78c}$$

and

$$\frac{\partial E_x}{\partial z} - \frac{\partial E_z}{\partial x} = -\mu\frac{\partial H_y}{\partial t} \tag{7.79a}$$

$$\frac{\partial H_y}{\partial x} = -\epsilon\frac{\partial E_x}{\partial t} \tag{7.79b}$$

$$\frac{\partial H_y}{\partial z} = -\epsilon\frac{\partial E_z}{\partial t} \tag{7.79c}$$

A similar analysis for shunt and series nodes in the x-y and y-z planes will yield the voltage-current equations and the corresponding Maxwell's equations. The three sets of two-dimensional shunt and series nodes oriented in the x-y, y-z, and z-x planes form a three-dimensional model. The two-dimensional nodes must be connected in such a way as to correctly describe Maxwell's equations at each three-dimensional node. Each of the shunt and series nodes has a spacing of $\Delta\ell/2$ so that like nodes are spaced $\Delta\ell$ apart.

Figure 7.23 illustrates a three-dimensional node representing a cubical volume of space $\Delta\ell/2$ long in each direction. A close examination shows that if the voltage
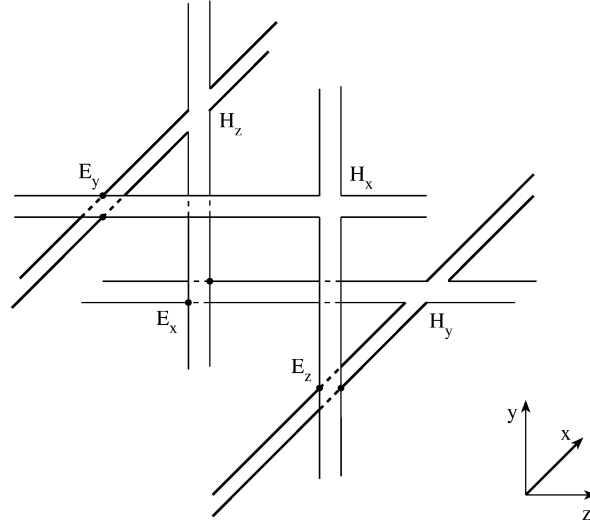

Figure 7.23

A three-dimensional node consisting of three shunt nodes and three series nodes.

between lines represents the **E** field and the current in the lines represents the **H** field, then the following Maxwell's equations are satisfied:

$$\frac{\partial H_x}{\partial z} - \frac{\partial H_z}{\partial x} = \epsilon \frac{\partial E_y}{\partial t} \tag{7.80a}$$

$$\frac{\partial E_z}{\partial y} - \frac{\partial E_y}{\partial z} = -\mu \frac{\partial H_x}{\partial t} \tag{7.80b}$$

$$\frac{\partial E_y}{\partial x} - \frac{\partial E_x}{\partial y} = -\mu \frac{\partial H_z}{\partial t} \tag{7.80c}$$

$$\frac{\partial E_x}{\partial z} - \frac{\partial E_z}{\partial x} = -\mu \frac{\partial H_y}{\partial t} \tag{7.80d}$$

$$\frac{\partial H_z}{\partial y} - \frac{\partial H_y}{\partial z} = \epsilon \frac{\partial E_x}{\partial t} \tag{7.80e}$$

$$\frac{\partial H_y}{\partial x} - \frac{\partial H_x}{\partial y} = \epsilon \frac{\partial E_z}{\partial t} \tag{7.80f}$$

In the upper half of the node in Fig. 7.23, we have a shunt node in the x-z plane (representing Eq. (7.80a)) connected to a series node in the y-z plane (representing Eq. (7.80b)) and a series node in the x-y plane (representing Eq. (7.80c)). In the lower half of the node, a series node in the x-z plane (representing Eq. (7.80d)) is connected to a shunt node in the y-z plane (representing Eq. (7.80e)) and a shunt node

in the x-y plane (representing Eq. (7.80f)). Thus Maxwell's equations are completely satisfied at the three-dimensional node. A three-dimensional TLM mesh is obtained by stacking similar nodes in x, y, and z directions (see Fig. 7.25, for example).

The wave characteristics of the three-dimensional mesh are similar to those of the two-dimensional mesh with the difference that low-frequency velocity is now $c/2$ instead of $c/\sqrt{2}$.

Figure 7.24 illustrates a schematic diagram of a three-dimensional node using single lines to represent pairs of transmission lines. It is more general than the representation in Fig. 7.23 in that it includes the permittivity, permeability, and loss stubs. Note that the dotted lines making up the corners of the cube are guidelines and do not represent transmission lines or stubs. It can be shown that for the general node the following equivalences apply [28]:

$$
\begin{aligned}
E_x &\equiv \text{ the common voltage at shunt node } E_x \\
E_y &\equiv \text{ the common voltage at shunt node } E_y \\
E_z &\equiv \text{ the common voltage at shunt node } E_z \\
H_x &\equiv \text{ the common current at series node } H_x \\
H_y &\equiv \text{ the common current at series node } H_y \\
H_z &\equiv \text{ the common current at series node } H_z \\
\epsilon_o &\equiv C \text{ (the capacitance per unit length of lines)} \\
\epsilon_r &\equiv 2\,(1 + Y_o/4) \\
\mu_o &\equiv L \text{ (the inductance per unit length of lines)} \\
\mu_r &\equiv 2\,(1 + Z_o/4) \\
\sigma &\equiv \frac{G_o}{\Delta\ell \frac{L}{C}}
\end{aligned}
\tag{7.81}
$$

where Y_o, Z_o, and G_o remain as defined in Sections 7.4 and 7.5. Interconnection of many of such three-dimensional nodes forms a TLM mesh representing any inhomogeneous media. The TLM method for three-dimensional problems is therefore concerned with applying Eq. (7.60) in conjunction with Eqs. (7.61) and (7.75) and obtaining the impulse response. Any of the field components may be excited initially by specifying initial impulses at the appropriate nodes. Also, the response at any node may be monitored by recording the pulses that pass through the node.

7.6.3 Boundary Conditions

Boundary conditions are simulated by short-circuiting shunt nodes (electric wall) or open-circuiting series nodes (magnetic wall) situated on a boundary. The tangential components of **E** must vanish in the plane of an electric wall, while the tangential components of **H** must be zero in the plane of a magnetic wall. For example, to set E_x and E_y equal to zero in a particular plane, all shunt nodes E_x and E_y lying in that plane are shorted. Similarly, to set H_y and H_z equal to zero in some plane, the series nodes H_y and H_z in that plane are simply open-circuited.

The continuity of the tangential components of **E** and **H** fields across a dielectric/dielectric boundary is automatically satisfied in the TLM mesh. For example,
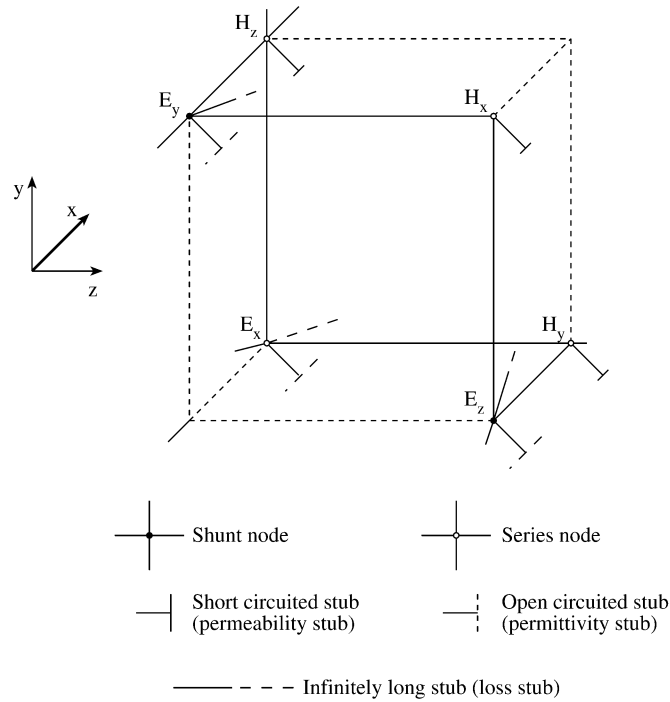
Figure 7.24
A general three-dimensional node.

for a dielectric/dielectric boundary in the x-z plane such as shown in Fig. 7.25, the following equations valid for a transmission-line element joining the nodes on either side of the boundaries are applicable:

$$E_{z1} = E_{z2} + \frac{\partial E_{z2}}{\partial y} \Delta \ell$$

$$E_{x1} = E_{x2} + \frac{\partial E_{x2}}{\partial y} \Delta \ell$$

$$H_{x1} = H_{x2} + \frac{\partial H_{x2}}{\partial y} \Delta \ell$$

$$H_{z1} = H_{z2} + \frac{\partial H_{z2}}{\partial y} \Delta \ell \qquad (7.82)$$

Finally, wall losses are included by introducing imperfect reflection coefficients as discussed in Section 7.5. The three-dimensional TLM mesh will be applied in solving the three-dimensional problems of resonant cavities in the following examples, taken from Akhtarzad and Johns [27].
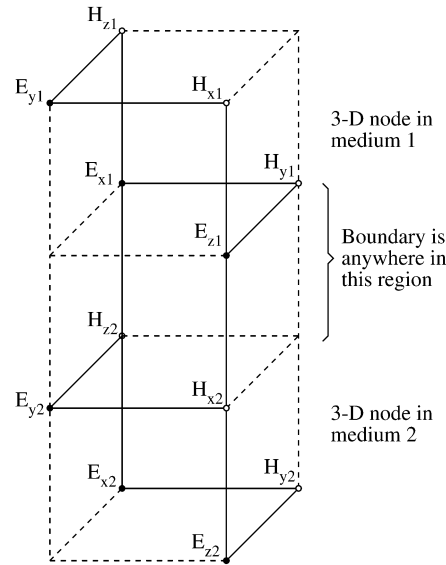
Figure 7.25
A dielectric/dielectric boundary in TLM mesh.

Example 7.5

Determine the resonant frequency of an $a \times b \times d$ empty rectangular cavity using the TLM method. Take $a = 12\Delta\ell$, $b = 8\Delta\ell$, and $d = 6\Delta\ell$. ⬚

Solution

The exact solution [13, 14] for TE$_{mnp}$ or TM$_{mnp}$ mode is

$$f_r = \frac{c}{2}\sqrt{(m/a)^2 + (n/b)^2 + (p/d)^2}$$

from which we readily obtain

$$k_c = \frac{w_r}{c} = \frac{2\pi f_r}{c} = \pi\sqrt{(m/a)^2 + (n/b)^2 + (p/d)^2}$$

The TLM program, the modified version of the program in [22], is shown in Fig. 7.26. The program initializes all field components by setting them equal to zero at all nodes in the $12\Delta\ell \times 8\Delta\ell \times 8\Delta\ell$ TLM mesh and exciting one field component. With subroutine COMPUTE, it applies Eq. (7.60) in conjunction with Eq. (7.61) and (7.75) to calculate the reflected **E** and **H** field components at all nodes. It applies the boundary conditions and calculates the impulse response at a particular node in the mesh.

The results of the computation along with the exact analytical values for the first few modes in the cavity are shown in Table 7.5. ▮

```
0001    C*****************************************************************
0002    C  THIS PROGRAM ANLYZES THREE-DIMENSIONAL WAVE PROBLEMS
0003    C  USING THE TLM METHOD
0004    C  THE SPECIFIC EXAMPLE SOLVED HERE IS THE DETERMINATION
0005    C  OF THE TM DOMINANT NODE OF RECTANGULAR LOSSLESS CAVITY
0006    C  OF DIMENSION 12 X 8 X 6
0007    C           E    ...  E - field
0008    C           H    ...  H - field
0009    C           X    ...  X - component
0010    C           Y    ...  Y - component
0011    C           Z    ...  Z - component
0012    C           I    ...  incident impulse
0013    C           R    ...  reflected impulse
0014    C           NX   ...  number of nodes in X-direction
0015    C           NY   ...  number of nodes in Y-direction
0016    C           NZ   ...  number of nodes in Z-direction
0017    C  SHUNT and SERIES  ...  scattering matrix
0018    C   DELTA = DELTA/LAMDA  (FREE SPACE)
0019
0020            IMPLICIT  REAL*8(A,B,D-H,O-Z),COMPLEX*8(C),
0021        1       INTEGER*2(I-N)
0022            DIMENSION EXR(2,7,9,13,5), EXI(2,7,9,13,5),
0023        1             EYR(2,7,9,13,5), EYI(2,7,9,13,5),
0024        2             EZR(2,7,9,13,5), EZI(2,7,9,13,5),
0025        3             HXR(2,7,9,13,5), HXI(2,7,9,13,5),
0026        4             HYR(2,7,9,13,5), HYI(2,7,9,13,5),
0027        5             HZR(2,7,9,13,5), HZI(2,7,9,13,5),
0028        6             EX(2,1000),EY(2,1000),EZ(2,1000),
0029        7             HX(2,1000),HY(2,1000),HZ(2,1000),
0030        8             OUT(12,1000),SHUNT(5,5),SERIES(5,5)
0031
0032            COMMON / PART1 /NT,NXB,NXE,NYB,NYE,NZB,NZE,IT
0033            SQMAG(CM) = ( CABS(CM) ) ** 2
0034            DATA ITRATE,NXB,NXE,NYB,NYE,NZB,NZE,NT,DELTA
0035        1       /1000, 1,  12, 1,  8,  1,  6,  4, 1.0/
0036            DATA NXI,NYI,NZI,NXO,NYO,NZO,RoH,NUMPT,DEL
0037        1       /11, 7,  0,  2,  2, 2,-1.0,1000,0.0001/
0038            DATA PI,        Eo,      Er, Ur,SIGMA,DELTA
0039        1       /3.1415927,8.854E-12,1.0,1.0,0.0,0.01 /
0040            DATA SERIES /-1.0,1.0,1.0,-1.0,-1.0,
0041        1             1.0,-1.0,-1.0,1.0,1.0,
0042        2             1.0,-1.0,-1.0,1.0,1.0,
0043        3             -1.0,1.0,1.0,-1.0,-1.0,
0044        4             -1.0,1.0,1.0,-1.0,-1.0/
0045            DATA SHUNT / 1.0,1.0,1.0,1.0,1.0,
0046        1             1.0,1.0,1.0,1.0,1.0,
0047        2             1.0,1.0,1.0,1.0,1.0,
0048        3             1.0,1.0,1.0,1.0,1.0,
0049        4             1.0,1.0,1.0,1.0,1.0/
0050
0051            Uo =  4.0 * PI * 1.0E-07
0052            Yo = 4.0 * (Er - 1.0)
0053            Zo = 4.0 * (Ur - 1.0)
0054            Go = SIGMA * DELTA * SQRT(Uo/Eo)
0055            Y = 4.0 + Yo + Go
0056            Z = 4.0 + Zo
0057            DO 5 I = 1,5
0058            SHUNT(I,5)  = SHUNT(I,5) * Yo
0059            SERIES(5,I) =  SERIES(5,I) * Zo
0060    5       CONTINUE
0061    C
```

Figure 7.26

Computer program for Example 7.5 *(Continued).*

```
0062    C  INITIALIZE ALL THE NODES
0063    C
0064           DO 10 IT = 1,2
0065           DO 10 K = NZB, NZE
0066           DO 10 J = NYB, NYE
0067           DO 10 I = NXB, NXE
0068           DO 10 L = 1, NT
0069              EXI(IT,K,J,I,L) = 0.0
0070              EYI(IT,K,J,I,L) = 0.0
0071              EZI(IT,K,J,I,L) = 0.0
0072              HXI(IT,K,J,I,L) = 0.0
0073              HYI(IT,K,J,I,L) = 0.0
0074              HZI(IT,K,J,I,L) = 0.0
0075              EXR(IT,K,J,I,L) = 0.0
0076              EYR(IT,K,J,I,L) = 0.0
0077              EZR(IT,K,J,I,L) = 0.0
0078              HXR(IT,K,J,I,L) = 0.0
0079              HYR(IT,K,J,I,L) = 0.0
0080    10        HZR(IT,K,J,I,L) = 0.0
0081    C
0082    C INSERT THE INITIAL EXCITATION
0083    C
0084           DO 15 K = NZB, NZE
0085           DO 15 L = 1, 4
0086              EZR(2,K,NYI,NXI,L) = 1.0
0087    15     CONTINUE
0088              IT = 2
0089    C
0090    C START ITERATION
0091    C
0092           DO 60 ITime = 1, ITRATE
0093              IF(ITIME .EQ. 1) GOTO 25
0094    C
0095    C COMPUTE THE REFLECTED E-FIELD AT ALL NODES
0096    C
0097              ISIGN = -1
0098              CALL COMPUTE(EXR,EYR,EZR,SHUNT
0099        1                    ,Y,EXI,EYI,EZI,ISIGN)
0100    C
0101    C RE-INITIALIZE MATRIX AND FORCE TANGENTIAL
0102    C E-FIELD TO ZERO AT BOUNDARY
0103    C
0104           DO 20 K = NZB, NZE
0105           DO 20 J = NYB, NYE
0106           DO 20 I = NXB, NXE
0107           DO 20 L = 1, NT
0108              HXI(IT-1,K,J,I,L) = 0.0
0109              HYI(IT-1,K,J,I,L) = 0.0
0110              HZI(IT-1,K,J,I,L) = 0.0
0111              IF(I .EQ. NXB) THEN
0112                 EYR(IT,K,J,I,L) = 0.0
0113                 EZR(IT,K,J,I,L) = 0.0
0114                 HXR(IT,K,J,I,L) = 0.0
0115              END IF
0116              IF(J .EQ. NYB)THEN
0117                 EXR(IT,K,J,I,L) = 0.0
0118                 EZR(IT,K,J,I,L) = 0.0
0119                 HYR(IT,K,J,I,L) = 0.0
0120              END IF
0121              IF(K .EQ. NZB)THEN
0122                 EXR(IT,K,J,I,L) = 0.0
0123                 EYR(IT,K,J,I,L) = 0.0
0124                 HZR(IT,K,J,I,L) = 0.0
```

Figure 7.26

(Cont.) **Computer program for Example 7.5 *(Continued).***

```
0125              END IF
0126      20      CONTINUE
0127      25      CONTINUE
0128              DO 30 K = NZB, NZE
0129              DO 30 J = NYB, NYE
0130              DO 30 I = NXB, NXE
0131            IF(J .NE. NYB)HZI(IT-1,K,J-1,I,4)=EXR(IT,K,J,I,1)
0132            IF(K .NE. NZB)HYI(IT-1,K-1,J,I,4)=EXR(IT,K,J,I,2)
0133                     HZI(IT-1,K,J,I,2)  =EXR(IT,K,J,I,3)
0134                     HYI(IT-1,K,J,I,2)  =EXR(IT,K,J,I,4)
0135            IF(I .NE. NXB)HZI(IT-1,K,J,I-1,3)=EYR(IT,K,J,I,1)
0136            IF(K .NE. NZB)HXI(IT-1,K-1,J,I,4)=EYR(IT,K,J,I,2)
0137                     HZI(IT-1,K,J,I,1)  =EYR(IT,K,J,I,3)
0138                     HXI(IT-1,K,J,I,2)  =EYR(IT,K,J,I,4)
0139            IF(I .NE. NXB)HYI(IT-1,K,J,I-1,3)=EZR(IT,K,J,I,1)
0140            IF(J .NE. NYB)HXI(IT-1,K,J-1,I,3)=EZR(IT,K,J,I,2)
0141                     HYI(IT-1,K,J,I,1)  =EZR(IT,K,J,I,3)
0142                     HXI(IT-1,K,J,I,1)  =EZR(IT,K,J,I,4)
0143      30      CONTINUE
0144      C
0145      C INSERT THE BOUNDARY CONDITIONS AT ALL BOUNDARIES
0146      C
0147              DO 35 K = NZB, NZE
0148              DO 35 J = NYB, NYE
0149              DO 35 I = NXB, NXE
0150                IF(I .EQ. NXB)THEN
0151                  HYI(IT-1,K,J,I,1) = RoH * HYR(IT,K,J,I,1)
0152                  HZI(IT-1,K,J,I,1) = RoH * HZR(IT,K,J,I,1)
0153                END IF
0154                IF(I .EQ. NXE)THEN
0155                  HZI(IT-1,K,J,I,3) = RoH * HZR(IT,K,J,I,3)
0156                  HYI(IT-1,K,J,I,3) = RoH * HYR(IT,K,J,I,3)
0157                END IF
0158                IF(J .EQ. NYB)THEN
0159                  HXI(IT-1,K,J,I,1) = RoH * HXR(IT,K,J,I,1)
0160                  HZI(IT-1,K,J,I,2) = RoH * HZR(IT,K,J,I,2)
0161                END IF
0162                IF(J .EQ. NYE)THEN
0163                  HXI(IT-1,K,J,I,3) = RoH * HXR(IT,K,J,I,3)
0164                  HZI(IT-1,K,J,I,4) = RoH * HZR(IT,K,J,I,4)
0165                END IF
0166                IF(K .EQ. NZB)THEN
0167                  HXI(IT-1,K,J,I,2) = RoH * HXR(IT,K,J,I,2)
0168                  HYI(IT-1,K,J,I,2) = RoH * HYR(IT,K,J,I,2)
0169                END IF
0170                IF(K .EQ. NZE)THEN
0171                  HXI(IT-1,K,J,I,4) = RoH * HXR(IT,K,J,I,4)
0172                  HYI(IT-1,K,J,I,4) = RoH * HYR(IT,K,J,I,4)
0173                END IF
0174      35      CONTINUE
0175      C
0176      C  COMPUTE THE H-FIELDS AT ALL THE NODES
0177      C
0178              ISIGN = 1
0179            CALL COMPUTE(HXR,HYR,HZR,SERIES,
0180          1                 Z,HXI,HYI,HZI,ISIGN)
0181      C
0182      C  RE-INITIALIZE ALL THE NODES
0183      C
0184              DO 40 K = NZB, NZE
0185              DO 40 J = NYB, NYE
0186              DO 40 I = NXB, NXE
0187              DO 40 L = 1, NT
```

Figure 7.26

(Cont.) **Computer program for Example 7.5** *(Continued).*

```
0188                    EXI(IT-1,K,J,I,L) = 0.0
0189                    EYI(IT-1,K,J,I,L) = 0.0
0190                    EZI(IT-1,K,J,I,L) = 0.0
0191     40        CONTINUE
0192               DO 45 K = NZB, NZE
0193               DO 45 J = NYB, NYE
0194               DO 45 I = NXB, NXE
0195                        EZI(IT-1,K,J,I,4)   =HXR(IT,K,J,I,1)
0196                        EYI(IT-1,K,J,I,4)   =HXR(IT,K,J,I,2)
0197            IF(J .NE. NYE)EZI(IT-1,K,J+1,I,2)=HXR(IT,K,J,I,3)
0198            IF(K .NE. NZE)EYI(IT-1,K+1,J,I,2)=HXR(IT,K,J,I,4)
0199                        EZI(IT-1,K,J,I,3)   =HYR(IT,K,J,I,1)
0200                        EXI(IT-1,K,J,I,4)   =HYR(IT,K,J,I,2)
0201            IF(I .NE. NXE)EZI(IT-1,K,J,I+1,1)=HYR(IT,K,J,I,3)
0202            IF(K .NE. NZE)EXI(IT-1,K+1,J,I,2)=HYR(IT,K,J,I,4)
0203                        EYI(IT-1,K,J,I,3)   =HZR(IT,K,J,I,1)
0204                        EXI(IT-1,K,J,I,3)   =HZR(IT,K,J,I,2)
0205            IF(I .NE. NXE)EYI(IT-1,K,J,I+1,1)=HZR(IT,K,J,I,3)
0206            IF(J .NE. NYE)EXI(IT-1,K,J+1,I,1)=HZR(IT,K,J,I,4)
0207     45        CONTINUE
0208     C
0209     C  CALCULATE THE IMPULSE RESPONSE AT NXO,NYO,NZO
0210     C
0211               EXT = 0.0
0212               EYT = 0.0
0213               EZT = 0.0
0214               HXT = 0.0
0215               HYT = 0.0
0216               HZT = 0.0
0217               DO 50 L = 1, NT
0218                  EXT = EXT + EXI(IT-1,NZO,NYO,NXO,L) * (2.0/Y)
0219                  EYT = EYT + EYI(IT-1,NZO,NYO,NXO,L) * (2.0/Y)
0220                  EZT = EZT + EZI(IT-1,NZO,NYO,NXO,L) * (2.0/Y)
0221                  HXT = HXT + HXI(IT-1,NZO,NYO,NXO,L) * (2.0/Y)
0222                  HYT = HYT + HYI(IT-1,NZO,NYO,NXO,L) * (2.0/Y)
0223     50           HZT = HZT + HZI(IT-1,NZO,NYO,NXO,L) * (2.0/Y)
0224     C
0225     C  SUM THE FREQUENCY RESPONSE(imaginary and real
0226     C  parts) FOR DIFFERENT VALUES OF MESH-SIZE DIVIDED
0227     C  BY WAVELENGTH BUT FIRST CONVOLVE IMPULSE RESPONSE
0228     C  WITH HANNING PROFILE
0229     C
0230               DINCR = DELTA
0231               DO 55 L = 1, NUMPT
0232                  T = DFLOAT(ITIME)
0233                  AMT = DFLOAT(ITRATE)
0234                  EXTH = EXT * (1.0 + DCOS(PI * T/AMT)) * 0.5
0235                  EYTH = EYT * (1.0 + DCOS(PI * T/AMT)) * 0.5
0236                  EZTH = EZT * (1.0 + DCOS(PI * T/AMT)) * 0.5
0237                  HXTH = HXT * (1.0 + DCOS(PI * T/AMT)) * 0.5
0238                  HYTH = HYT * (1.0 + DCOS(PI * T/AMT)) * 0.5
0239                  HZTH = HZT * (1.0 + DCOS(PI * T/AMT)) * 0.5
0240            EX(1,L) = EX(1,L) + EXTH * DCOS(2.0*PI*T*DINCR)
0241            EX(2,L) = EX(2,L) + EXTH * DSIN(2.0*PI*T*DINCR)
0242            EY(1,L) = EY(1,L) + EYTH * DCOS(2.0*PI*T*DINCR)
0243            EY(2,L) = EY(2,L) + EYTH * DSIN(2.0*PI*T*DINCR)
0244            EZ(1,L) = EZ(1,L) + EZTH * DCOS(2.0*PI*T*DINCR)
0245            EZ(2,L) = EZ(2,L) + EZTH * DSIN(2.0*PI*T*DINCR)
0246            HX(1,L) = HX(1,L) + HXTH * DCOS(2.0*PI*T*DINCR)
0247            HX(2,L) = HX(2,L) + HXTH * DSIN(2.0*PI*T*DINCR)
0248            HY(1,L) = HY(1,L) + HYTH * DCOS(2.0*PI*T*DINCR)
0249            HY(2,L) = HY(2,L) + HYTH * DSIN(2.0*PI*T*DINCR)
```

Figure 7.26

(Cont.) **Computer program for Example 7.5** *(Continued).*

```
0250                HZ(1,L) = HZ(1,L) + HZTH * DCOS(2.0*PI*T*DINCR)
0251                HZ(2,L) = HZ(2,L) + HZTH * DSIN(2.0*PI*T*DINCR)
0252                  OUT(1,L) = DINCR
0253      55         DINCR = DINCR + DEL
0254      60      CONTINUE
0255             DO L = 1, NUMPT
0256                CEX = CMPLX(EX(1,L),EX(2,L))
0257                CEY = CMPLX(EY(1,L),EY(2,L))
0258                CEZ = CMPLX(EZ(1,L),EZ(2,L))
0259                CHX = CMPLX(HX(1,L),HX(2,L))
0260                CHY = CMPLX(HY(1,L),HY(2,L))
0261                CHZ = CMPLX(HZ(1,L),HZ(2,L))
0262                OUT(2,L) = CABS(CEX)
0263                OUT(3,L) = CABS(CEY)
0264                OUT(4,L) = CABS(CEZ)
0265                OUT(5,L) = CABS(CHX)
0266                OUT(6,L) = CABS(CHY)
0267                OUT(7,L) = CABS(CHZ)
0268          OUT(8,L)=SQRT(SQMAG(CEX)+SQMAG(CEY)+SQMAG(CEZ))
0269          OUT(9,L)=SQRT(SQMAG(CHX)+SQMAG(CHY)+SQMAG(CHZ))
0270                END DO
0271      C
0272      C  PICK THE MODES
0273      C
0274             DO 65 L = 2, 9
0275             DO 65 K = 1, NUMPT
0276                IF(K .NE. 1 .AND. K .NE. NUMPT) THEN
0277                   IF(OUT(L,K) .GT. OUT(L,K-1) .AND.
0278      1              OUT(L,K) .GT. OUT(L,K+1)) THEN
0279                      WRITE(6,80) L,K,(OUT(J,K),J=1,9)
0280                   END IF
0281                END IF
0282      65     CONTINUE
0283      C
0284      C  WRITE OUT DATA FOR PLOTTING
0285      C
0286             DO 70 L = 2, 9
0287             DO 70 K = 1, NUMPT
0288             WRITE(6,75) K, OUT(1,K), OUT(L,K)
0289      70     CONTINUE
0290      75     FORMAT(I5,4F15.8)
0291      80     FORMAT(2I5,10F8.4)
0292             STOP
0293             END

0001      C*************************************************
0002      C  THIS SUBROUTINE COMPUTES THE REFLECTED PULSES
0003      C
0004             SUBROUTINE COMPUTE(AXR,AYR,AZR,SCATTER,
0005      1                         W,AXI,AYI,AZI,ISIGN)
0006             IMPLICIT REAL*8(A-H,O-Z), INTEGER*2(I-N)
0007             DIMENSION AXR(2,NZE,NYE,NXE,NT),
0008      1       AYR(2,NZE,NYE,NXE,NT),SCATTER(5,5),
0009      2       AZR(2,NZE,NYE,NXE,NT),AXI(2,NZE,NYE,NXE,NT),
0010      3        AYI(2,NZE,NYE,NXE,NT),AZI(2,NZE,NYE,NXE,NT)
0011
0012             COMMON / PART1 /NT,NXB,NXE,NYB,NYE,NZB,NZE,IT
0013
0014             DO 20 K = NZB, NZE
0015             DO 20 J = NYB, NYE
0016             DO 20 I = NXB, NXE
0017      C   INSERT FEW LINES HERE FOR INHOMOGENEOUS CAVITY
0018                DO 15 L = 1, NT
```

Figure 7.26

(Cont.) **Computer program for Example 7.5** *(Continued).*

```
0019              AXRS = 0.0
0020              AYRS = 0.0
0021              AZRS = 0.0
0022              DO 10 M = 1, NT
0023          AXRS = AXRS+2./W*SCATTER(L,M)*AXI(IT-1,K,J,I,M)
0024          AYRS = AYRS+2./W*SCATTER(L,M)*AYI(IT-1,K,J,I,M)
0025          AZRS = AZRS+2./W*SCATTER(L,M)*AZI(IT-1,K,J,I,M)
0026      10      CONTINUE
0027          AXR(IT,K,J,I,L)=AXRS+ISIGN*AXI(IT-1,K,J,I,L)
0028          AYR(IT,K,J,I,L)=AYRS+ISIGN*AYI(IT-1,K,J,I,L)
0029          AZR(IT,K,J,I,L)=AZRS+ISIGN*AZI(IT-1,K,J,I,L)
0030      15      CONTINUE
0031      20    CONTINUE
0032            RETURN
0033            END
```

Figure 7.26
(Cont.) **Computer program for Example 7.5.**

Table 7.5   Resonant Wavenumber $(k_c a)$ of an
Empty Rectangular Cavity, where $k_c a = 4\pi a/c$ and
λ is the Free-space Wavelength

Modes	Exact results	TLM results	Error %
TM_{110}	5.6636	5.6400	0.42
TE_{101}	7.0249	6.9819	0.61
TM_{210}, TE_{011}	7.8540	7.8112	0.54

Example 7.6

Modify the TLM program in Fig. 7.26 to calculate the resonant wavenumber $k_c a$ of the inhomogeneous cavities in Fig. 7.27. Take $\epsilon_r = 16, a = \Delta\ell, b = 3a/10, d = 4a/10, s = 7a/12.$ []

Solution

The main program in Fig. 7.26 is applicable to this example. Only the subroutine COMPUTE requires slight modification to take care of the inhomogeneity of the cavity. The modifications in the subprogram for the cavities in Fig. 7.27 (a) and (b) are shown in Fig. 7.28 (a) and (b), respectively. For each modification, the few lines in Fig. 7.28 are inserted in between lines 15 and 17 in subroutine COMPUTE of Fig. 7.26. The results are shown in Table 7.6 for TE_{101} mode.   ▮
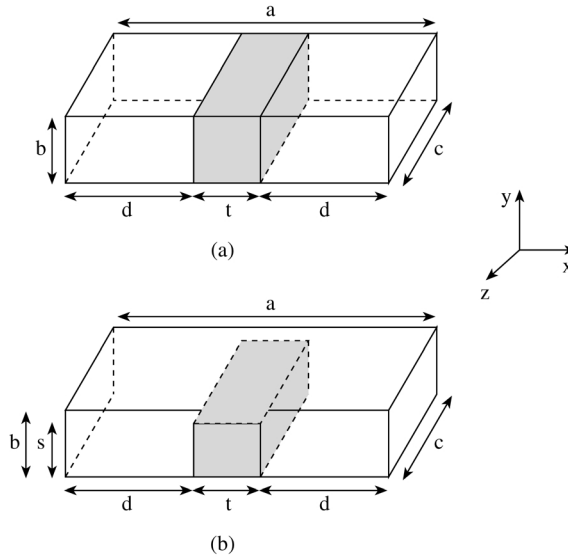
Figure 7.27

Rectangular cavity loaded with dielectric slab.

```
        :
        :
        :

0001    C*************************************************
0002    C   THIS SUBROUTINE COMPUTES THE REFLECTED PULSES
0003    C
0004            SUBROUTINE COMPUTE(AXR,AYR,AZR,SCATTER,
0005       1                       WW,AXI,AYI,AZI,ISIGN)

        :
        :
        :

0017    C   INSERT FEW LINES HERE FOR INHOMOGENEOUS CAVITY
0018        IF ((I.GE.9).AND.(I.LE.13)
0019       1              .AND.(ISIGN.EQ.-1)) THEN
0020          NT = 5
0021          W = WW
0022                    ELSE
0023          NT = 4
0024          W = 4.0
0025          END IF

        :
        :
        :
```

Figure 7.28

(a) Modification in subroutine COMPUTE for the inhomogeneous cavity of [Fig. 7.27 (a)](#) *(Continued).*

```
0001    C*********************************************
0002    C  THIS SUBROUTINE COMPUTES THE REFLECTED PULSES
0003    C
0004          SUBROUTINE COMPUTE(AXR,AYR,AZR,SCATTER,
0005     1                       WW,AXI,AYI,AZI,ISIGN)
   .
   .
   .
0017    C  INSERT FEW LINES HERE FOR INHOMOGENEOUS CAVITY
0018          IF (J.GT.4) GO TO 5
0019          IF ((I.GE.9).AND.(I.LE.13)
0020     1                 .AND.(ISIGN.EQ.-1)) THEN
0021        NT = 5
0022        W = WW
0023            GO TO 6
0024        END IF
0025     5  CONTINUE
0026        NT = 4
0027        W = 4.0
0028     6  CONTINUE
0029            DO 15 L = 1, NT
   .
   .
   .
```

Figure 7.28
(Cont.) **(b) Modification in subroutine COMPUTE for the inhomogeneous cavity of Fig. 7.27 (b).**

Table 7.6 Resonant Wavenumber ($k_c a$) for TE$_{101}$ Mode of Inhomogeneous Rectangular Cavities, where $k_c a = 4\pi a/c$, and λ is the Free-space Wavelength

Modes	Exact results	TLM results	Error %
Fig. 7.27 (a)	2.589	2.5761	0.26
Fig. 7.27 (b)	(none)	3.5387	

7.7 Error Sources and Correction

As in all approximate solutions such as the TLM technique, it is important that the error in the final result be minimal. In the TLM method, four principal sources of error can be identified [10, 28, 29]:

- truncation error,

- coarseness error,

- velocity error,

- misalignment error.

Each of these sources of error and ways of minimizing it will be discussed.

7.7.1 Truncation Error

The truncation error is due to the need to truncate the impulse response in time. As a result of the finite duration of the impulse response, its Fourier transform is not a line spectrum but rather a superposition of $\sin x/x$ functions, which may interfere with each other and cause a slight shift in their maxima. The maximum truncation error is given by

$$e_T = \frac{\Delta S}{\Delta \ell / \lambda c} = \frac{3\lambda_c}{SN^2\pi^2\Delta\ell} \tag{7.83}$$

where λ_c is the cutoff wavelength to be calculated, ΔS is the absolute error in $\Delta\ell/\lambda_c$, S is the frequency separation (expressed in terms of $\Delta\ell/\lambda_c$, λ_c being the free-space wavelength) between two neighboring peaks as shown in Fig. 7.29, and N is the number of iterations. Equation (7.83) indicates that e_T decreases with increasing N and increasing S. It is therefore desirable to make N large and suppress all unwanted modes close to the desired mode by carefully selecting the input and output points in the TLM mesh. An alternative way of reducing the truncation error is to use a Hanning window in the Fourier transform. For further details on this, one should consult [10, 31].
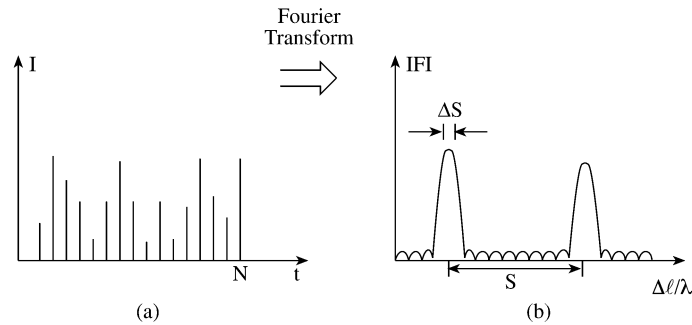
Figure 7.29

Source of truncation error: (a) Truncated output impulse, (b) resulting truncation error in the frequency domain.

7.7.2 Coarseness Error

This occurs when the TLM mesh is too coarse to resolve highly nonuniform fields as can be found at corners and edges. An obvious solution is to use a finer mesh

$(\Delta \ell \rightarrow 0)$, but this would lead to large memory requirements and there are limits to this refinement. A better approach is to use variable mesh size so that a higher resolution can be obtained in the nonuniform field region [71]. This approach requires more complicated programming.

7.7.3 Velocity Error

This stems from the assumption that propagation velocity in the TLM mesh is the same in all directions and equal to $u_n = u/\sqrt{2}$, where u is the propagation velocity in the medium filling the structure. The assumption is only valid if the wavelength λ_n in the TLM mesh is large compared with the mesh size $\Delta \ell (\Delta \ell / \lambda_n < 0.1)$. Thus the cutoff frequency f_{cn} in the TLM mesh is related to the cutoff frequency f_c of the real structure according to $f_c = f_{cn} \sqrt{2}$. If $\Delta \ell$ is comparable with λ_n, the velocity of propagation depends on the direction and the assumption of constant velocity results in a velocity error in f_c. Fortunately, a measure to reduce the coarseness error takes care of the velocity error as well.

7.7.4 Misalignment Error

This error occurs in dielectric interfaces in three-dimensional inhomogeneous structures such as microstrip or fin line. It is due to the manner in which boundaries are simulated in a three-dimensional TLM mesh; dielectric interfaces appear halfway between nodes, while electric and magnetic boundaries appear across such nodes. If the resulting error is not acceptable, one must make two computations, one with recessed and one with protruding dielectric, and take the average of the results.

7.8 Absorbing Boundary Conditions

Just like FDTD and FEM, the TLM method requires absorbing boundary conditions (ABCs) at the limit of the solution region. Several ABCs have proposed for TLM simulations [32]–[37]. It has been recognized that the perfectly matched-layer (PML) technique, discussed for FDTD in Section 3.9, has excellent absorbing performances that are significantly superior to other techniques. So only PML will be discussed here.

Consider the PML region and the governing Maxwell's equations. Each field component is split into two. For example, $E_x = E_{xy} + E_{xz}$. In 3-D, Maxwell's

equations become twelve [38]:

$$\mu_o \frac{H_{xy}}{\partial t} + \sigma_y^* H_{xy} = -\frac{\partial(E_{zx} + E_{zy})}{\partial y} \tag{7.84a}$$

$$\mu_o \frac{H_{xz}}{\partial t} + \sigma_z^* H_{xz} = \frac{\partial(E_{yx} + E_{yz})}{\partial z} \tag{7.84b}$$

$$\mu_o \frac{H_{yz}}{\partial t} + \sigma_z^* H_{yz} = -\frac{\partial(E_{xy} + E_{xz})}{\partial z} \tag{7.84c}$$

$$\mu_o \frac{H_{yx}}{\partial t} + \sigma_x^* H_{yx} = \frac{\partial(E_{zx} + E_{zy})}{\partial x} \tag{7.84d}$$

$$\mu_o \frac{H_{zx}}{\partial t} + \sigma_x^* H_{zx} = -\frac{\partial(E_{yx} + E_{yz})}{\partial x} \tag{7.84e}$$

$$\mu_o \frac{H_{zy}}{\partial t} + \sigma_y^* H_{zy} = \frac{\partial(E_{xy} + E_{xz})}{\partial y} \tag{7.84f}$$

$$\epsilon_o \frac{E_{xy}}{\partial t} + \sigma_y E_{xy} = \frac{\partial(H_{zx} + H_{zy})}{\partial y} \tag{7.84g}$$

$$\epsilon_o \frac{E_{xz}}{\partial t} + \sigma_z E_{xz} = -\frac{\partial(H_{yx} + H_{yz})}{\partial z} \tag{7.84h}$$

$$\epsilon_o \frac{E_{yz}}{\partial t} + \sigma_z E_{yz} = \frac{\partial(H_{xy} + H_{xz})}{\partial z} \tag{7.84i}$$

$$\epsilon_o \frac{E_{yx}}{\partial t} + \sigma_x E_{yx} = -\frac{\partial(H_{zx} + H_{zy})}{\partial x} \tag{7.84j}$$

$$\epsilon_o \frac{E_{zx}}{\partial t} + \sigma_x E_{zx} = \frac{\partial(H_{yx} + H_{yz})}{\partial x} \tag{7.84k}$$

$$\epsilon_o \frac{E_{zy}}{\partial t} + \sigma_y E_{zy} = -\frac{\partial(H_{xy} + H_{xz})}{\partial y} \tag{7.84l}$$

in which (σ_i, σ_i^*) where $i \in \{x, y, z\}$ are, respectively, the electric and magnetic conductivities of the PML region and they satisfy

$$\frac{\sigma_i}{\epsilon_o} = \frac{\sigma_i^*}{\mu_o} \tag{7.85}$$

Using the usual Yees's notation, the field samples are expressed as

$$E_x^n(i, j, k) = E_x[(i + 1/2)\delta, j\delta, k\delta, (n + 1/2)\delta t]$$
$$E_y^n(i, j, k) = E_y[i\delta, (j + 1/2)\delta, k\delta, (n + 1/2)\delta t]$$
$$E_z^n(i, j, k) = E_z[i\delta, j\delta, (k + 1/2)\delta, (n + 1/2)\delta t]$$
$$H_x^n(i, j, k) = H_x[i\delta, (j + 1/2)\delta, (k + 1/2)\delta, n\delta t]$$
$$H_y^n(i, j, k) = H_y[(i + 1/2)\delta, j\delta, (k + 1/2)\delta, n\delta t]$$
$$H_z^n(i, j, k) = H_z[(i + 1/2)\delta, (j + 1/2)\delta, k\delta, n\delta t] \tag{7.86}$$

where $\delta = \Delta x = \Delta y = \Delta z = \Delta \ell$. Without loss of generality, we set $\delta t = \delta/2c$. Since we want to interface the FDTD algorithm with the TLM, we express the fields

in terms of voltages. For a cubic cell,

$$V_{ers}^n(i, j, k) = \delta E_{rs}^n(i, j, k) \quad \text{with } r \in \{x, y\}, \quad s \in \{x, z\} \tag{7.87a}$$

$$V_{ms}^n(i, j, k) = \sqrt{\frac{\mu_o}{\epsilon_o}} \delta H_s^n(i, j, k) \quad \text{with } s \in \{y, z\} \tag{7.87b}$$

where the subscripts e and m denote electric and magnetic, respectively. By applying the central-difference scheme to Eq. (7.84), we obtain after some algebraic manipulations

$$V_{exy}^n(i, j, k) = \left(\frac{4 - G_{ey}}{4 + G_{ey}}\right) V_{exy}^{n-1}(i, j, k)$$

$$+ \left(\frac{2}{4 + G_{ey}}\right) \left(V_{mz}^n(i, j, k) - V_{mz}^n(i, j - 1, k)\right) \tag{7.88a}$$

$$V_{exz}^n(i, j, k) = \left(\frac{4 - G_{ez}}{4 + G_{ez}}\right) V_{exz}^{n-1}(i, j, k)$$

$$- \left(\frac{2}{4 + G_{ez}}\right) \left(V_{my}^n(i, j, k) - V_{my}^n(i, j, k - 1)\right) \tag{7.88b}$$

$$V_{ex}^n(i, j, k) = V_{exy}^n(i, j, k) + V_{exz}^n(i, j, k) \tag{7.88c}$$

where $G_{es} = \delta\sigma_s(i, j, k)\sqrt{\mu_o\epsilon_o}$ with $s \in \{y, z\}$. Applying this TLM FDTD-PML algorithm has been found to yield excellent performance with reflection level below -55 dB [37].

7.9 Concluding Remarks

This chapter has described the transmission-line-matrix (TLM) method which is a modeling process rather than a numerical method for solving differential or equations. The flexibility, versatility, and generality of the time-domain method have been demonstrated. Our discussion in this chapter has been introductory, and one is advised to consult [10], [39]–[41] for a more in-depth treatment. A generalized treatment of TLM in the curvilinear coordinate system is presented in [42], while a theoretical basics of TLM is derived in [43]. Further developments in TLM can be found in [44]–[50].

Although the application of the TLM method in this chapter has been limited to diffusion and wave propagation problems, the method has a wide range of applications. The technique has been applied to other problems such as:

- cutoff frequencies in fin lines [29, 30],

- transient analysis of striplines [51, 52],

- linear and nonlinear lumped networks [53]–[58],

- microstrip lines and resonators [17, 59, 60],

- diffusion problems [61]–[63],

- electromagnetic compatibility problems [21], [64]–[67],

- antenna problems [43, 53, 68, 69],

- induced currents in biological bodies exposed to EM fields [70],

- cylindrical and spherical waves [53, 71, 72], and

- others [73]–[78].

A major advantage of the TLM method, as compared with other numerical techniques, is the ease with which even the most complicated structures can be analyzed. The great flexibility and versatility of the method reside in the fact that the TLM mesh incorporates the properties of EM fields and their interaction with the boundaries and material media. Hence, the EM problem need not be formulated for every new structure. Thus a general-purpose program such as in [79] can be developed such that only the parameters of the structure need be entered for computation. Another advantage of using the TLM method is that certain stability properties can be deduced by inspection of the circuit. There are no problems with convergence, stability or spurious solutions. The method is limited only by the amount of memory storage required, which depends on the complexity of the TLM mesh. Also, being an explicit numerical solutions, the TLM method is suitable for nonlinear or inhomogeneous problems since any variation of material properties may be updated at each time step.

Perhaps the best way to conclude this chapter is to compare the TLM method with the finite difference method, especially FDTD [80]–[86]. While TLM is a physical model based on Huygens' principle using interconnected transmission lines, the FDTD is an approximate mathematical model directly based on Maxwell's equations. In the two-dimensional TLM, the magnetic and electric field components are located at the same position with respect to space and time, whereas in the corresponding two-dimensional FDTD cell, the magnetic field components are shifted by half an interval in space and time with respect to the electric field components. Due to this displacement between electric and magnetic field components in Yee's FDTD, Chen et al. [83] derived a new FDTD and demonstrated that the new FDTD formulation is exactly equivalent to the symmetric condensed node model used in the TLM method. This implies that the TLM algorithm can be formulated in FDTD form and vice versa. However, both algorithms retain their unique advantages. For example, the FDTD model has a simpler algorithm where constitutive parameters are directly introduced, while the TLM has certain advantages in the modeling of boundaries and the partitioning of the solution region. Furthermore, the FDTD requires less than one-half of the CPU time spent by the equivalent TLM program under identical conditions. While the TLM scheme requires 22 real memory stores per node, the FDTD method requires only seven real memory stores per 3-D node in an isotropic dielectric medium [81].

Although both are time-domain schemes, the quantities available at each time step are the solution in TLM model and there is no need for an iterative procedure. The dispersion relations for TLM and FDTD are identical for 2-D but are different for 3-D problems. The comparison is summarized in Table 7.7. According to Johns, the two methods complement each other rather than compete with each other [80].

Table 7.7   A Comparison of TLM and FDTD Methods

FDTD	TLM
A mathematical model based on Maxwell's equations	A physical model based on Huygen's principle
E and H are shifted with respect to space and time	E and H are calculated at the same time and position
Requires less memory and one-half the CPU time	Needs more memory and more CPU time
Provides solution at each time step	Requires some iterative procedure

References

[1] G. Kron, "Numerical solution of ordinary and partial differential equations by means of equivalent circuits," *J. Appl. Phys.,* Vol. 16, Mar. 1945, pp. 172–186.

[2] C.H. Durney and C.C. Johnson, *Introduction to Modern Electromagnetics.* New York: McGraw-Hill, 1969, pp. 286–287.

[3] P.P. Silvester and F.L. Ferrari, *Finite Elements for Electrical Engineers.* Cambridge: Cambridge University Press, 1983, p. 24.

[4] R.H. Park, "Definition of an ideal synchronous machine and formulators for armature flux linkages," *Gen. Elect. Rev.,* vol. 31, 1928, pp. 332–334.

[5] G. Kron, "Equivalent circuit of the field equations of Maxwell," *Proc. IRE,* May 1944, pp. 289–299.

[6] G. Kron, *Equivalent Circuits os Electrical Machinery.* New York: John Wiley, 1951.

[7] N. Marcovitz and J. Schwinger, "On the reproduction of the electric and magnetic fields produced by currents and discontinuity in wave guides, I," *J. Appl. Phys.,* vol. 22, no. 6, June 1951. pp. 806–819.

[8] J. Schwinger and D.S. Saxon, *Discontinuities in Waveguides.* New York: Gordon and Breach, 1968.

[9] P.B. Johns and R.L. Beurle, "Numerical solution of 2-dimensional scattering problems using a transmission line matrix," *Proc. IEEE,* vol. 118, no. 9, Sept. 1971, pp. 1203–1208.

[10] W.J.R. Hoefer, "The transmission-line matrix method—theory and applications," *IEEE Trans. Microwave Theory Tech.,* vol. MTT-33, no. 10, Oct. 1985, pp. 882–893.

[11] C. Christopoulos, *The Transmission-Line Modeling Method (TLM).* New York: IEEE Press, 1995.

[12] M.N.O. Sadiku and L.C. Agba, "A simple introduction to the transmission-line modeling," *IEEE Trans. Cir. Sys.,* vol. CAS-37, no. 8, Aug. 1990, pp. 991–999.

[13] B.J. Ley, *Computer Aided Analysis and Design for Electrical Engineers.* New York: Holt, Rinehart and Winston, 1970, pp. 815–817.

[14] M.N.O. Sadiku, *Elements of Electromagnetics.* New York: Oxford Univ. Press, 2nd ed., 1992, pp. 518–592.

[15] C.C. Wong, "Solution of the network analog of one-dimensional field equations using the ladder method," *IEEE Trans. Educ.,* vol. E-28, no. 3, Aug. 1985, pp. 176–179.

[16] C.C. Wong and W.S. Wong, "Multigrid TLM for diffusion problems," *Int. J. Num. Model.,* vol. 2, no. 2, 1989, pp. 103–111.

[17] G.E. Marike and G. Yek, "Dynamic three-dimensional T.L.M. analysis of microstrip lines on anisotropic substrate," *IEEE Trans. Micro. Theo. Tech.,* vol. MTT-33, no. 9, Sept. 1985, pp. 789–799.

[18] P.B. Johns, "Applications of the transmission-line matrix method to homogeneous waveguides of arbitrary cross-section," *Proc. IEEE,* vol. 119, no. 8, Aug. 1972, pp. 1086–1091.

[19] R.A. Waldron, *Theory of Guided Electromagnetic Waves.* London: Van Nostrand Reinhold Co., 1969, pp. 157–172.

[20] N.R.S. Simons and E. Bridges, "Method for modeling free space boundaries in TLM situations," *Elect. Lett.,* vol. 26, no. 7, March 1990, pp. 453–455.

[21] C. Christopoulos and J.L. Herring, "The application of the transmission-line modeling (TLM) to electromagnetic compatibility problems," *IEEE Trans. Elect. Magn. Comp.,* vol. 35, no. 2, May 1993, pp. 185–191.

[22] L.C. Agba, "Transmission-line-matrix modeling of inhomogeneous rectangular waveguides and cavities," M.S. thesis, Department of Electrical and Computer Engr., Florida Atlantic University, Boca Raton, Aug. 1987.

[23] P.B. Johns, "The solution of inhomogeneous waveguide problems using a transmission line matrix," *IEEE Trans. Micro. Theo. Tech.,* vol. MTT-22, no. 3, Mar. 1974, pp. 209–215.

[24] S. Akhtarzad and P.B. Johns, "Generalized elements for t.l.m. method of numerical analysis," *Proc. IEEE,* vol. 122, no. 12, Dec. 1975, pp. 1349–1352.

[25] S. Akhtarzad and P.B. Johns, "Numerical solution of lossy waveguides: T.L.M. computer programs," *Elec. Lett.,* vol. 10, no. 15, July 25, 1974, pp. 309–311.

[26] S. Akhtarzad and P.B. Johns, "Transmission line matrix solution of waveguides with wall losses," *Elec. Lett.,* vol. 9, no. 15, July 1973, pp. 335–336.

[27] S. Akhtarzad and P.B. Johns, "Solution of Maxwell's equations in three space dimensional and time by the T.L.M. method of numerical analysis," *Proc. IEEE,* vol. 122, no. 12, Dec. 1975, pp. 1344–1348.

[28] S. Akhtarzad and P.B. Johns, "Three-dimensional transmission-line Matrix computer analysis of microstrip resonators," *IEEE Trans. Micro. Theo. Tech.,* vol. MTT-23, no. 12, Dec. 1975, pp. 990–997.

[29] Y.C. Shih and W.J.R. Hoefer, "The accuracy of TLM analysis of finned rectangular waveguides," *IEEE Trans. Micro. Theo. Tech.,* vol. MTT-28, no. 7, July 1980, pp. 743–746.

[30] Y.C. Shih and W.J.R. Hoefer, "Dominant and second-order mode cutoff frequencies in fin lines calculated with a two-dimensional TLM program," *IEEE Trans. Micro. Theo. Tech.,* vol. MTT-28, no. 12, Dec. 1980, pp. 1443–1448.

[31] N. Yoshida, et al., "Transient analysis of two-dimensional Maxwell's equations by Bergeron's method," *Trans. IECE* (Japan), vol. J62B, June 1979, pp. 511–518.

[32] J.A. Morente and J.A. Porti, and M. Khalladi, "Absorbing boundary conditions for the TLM method," *IEEE Trans. Micro. Theo. Tech.,* vol. 40, no. 11, Nov. 1992, pp. 2095–2099.

[33] S.C. Pomeroy, G. Zhang, and C. Wykes, "Variable coefficient absorbing boundary condition for TLM," *Elect. Lett.,* vol. 29, no. 13, June 1993, pp. 1198–1200.

[34] C. Eswarappa and W.J.R. Hoefer, "One-way equation absorbing boundary conditions for 3-D TLM analysis of planar and quasi-planar structures," *IEEE Trans. Micro. Theo. Tech.,* vol. 42, no. 9, Sept. 1994, pp. 1669–1677.

[35] N. Kukutsu and R. Konno, "Super absorption boundary conditions for guided waves in the 3-D TLM simulation," *IEEE Micro. Guided Wave Lett.,* vol. 5, Sept. 1995, pp. 299–301.

[36] N. Pena and M.M. Ney, "A new TLM node for Berenger's perfectly matched layer (PML)," *IEEE Micro. Guided Wave Lett.,* vol. 6, Nov. 1996, pp. 410–412.

[37] N. Pena and M.M. Ney, "Absorbing-boundary conditions using perfectly matched-layer (PML) technique for three-dimensional TLM simulations," *IEEE Trans. Micro. Theo. Tech.,* vol. 45, no. 10, Oct. 1997, pp. 1749–1755.

[38] A. Taflove, *Computational Electrodynamics.* Boston, MA: Artech House, 1995, pp. 189–190.

[39] P.B. Johns. "Numerical modeling by the TLM method," in A. Wexler (ed.), *Large Engineering Systems.* Oxford: Pergamon, 1977.

[40] T. Itoh (ed.), *Numerical Techniques for Microwave and Millimeterwave Passive Structure.* New York: John Wiley, 1989, pp. 496–591.

[41] P.B. Johns, "Simulation of electromagnetic wave interactions by transmission-line modeling (TLM)," *Wave Motion,* vol. 10, no. 6, 1988, pp. 597–610.

[42] A.K. Bhattacharyya and R. Garg, "Generalized transmission line model for microstrip patches," *IEEE Proc.,* vol. 132, Pt. H, no. 2, April 1985, pp. 93–98.

[43] M. Krumpholz and P. Russer, "A field theoretical derivation of TLM," *IEEE Trans. Micro. Theo. Tech.,* vol. 42, no. 9, Sept. 1994, pp. 1660–1668.

[44] P. Naylor and C. Christopoulos, "A comparison between the time-domain and the frequency-domain diakopic methods of solving field problems by transmission-line modeling," *Int. Jour. Num. Model.,* vol. 2, no. 1, 1989, pp. 17–30.

[45] P. Saguet, "The 3-D transmission-line matrix method theory and comparison of the processes," *Int. Jour. Num. Model.,* vol. 2, 1989, pp. 191–201.

[46] W.J.R. Hoefer, "The discrete time domain Green's function or Johns matrix — a new powerful concept in transmission line modeling (TLM)," *Int. Jour. Num. Model.,* vol. 2, no. 4, 1989, pp. 215–225.

[47] L.R.A.X. de Menezes and W.J.R. Hoefer, "Modeling of general constitutive relationship in SCN TLM," *IEEE Trans. Micro. Theo. Tech.,* vol. 44, no. 6, June 1996, pp. 854–861.

[48] V. Trenkic, C. Christopoulos, and T.M. Benson, "Simple and elegant formulation of scattering in TLM nodes," *Elec. Lett.,* vol. 29, no. 18, Sept. 1993, pp. 1651–1652.

[49] J.L. Herring and C. Christopoulos, "Solving electromagnetic field problems using a multiple grid transmission-line modeling method," *IEEE Trans. Ant. Prop.,* vol. 42, no. 12, Dec. 1994, pp. 1655–1658.

[50] J.A. Porti, J.A. Morente, and M.C. Carrion, "Simple derivation of scattering matrix for TLM nodes," *Elect. Lett.,* vol. 34, no. 18, Sept. 1998, pp. 1763–1764.

[51] N. Yoshida, I. Fukai, and J. Fukuoka, "Transient analysis of three-dimensional electromagnetic fields by nodal equations," *Trans. Inst. Electron. Comm. Engr. Japan,* vol. J63B, Sept. 1980, pp. 876–883.

[52] N. Yoshida and I. Fukai, "Transient analysis of a stripline having corner in three-dimensional space," *IEEE Trans. Micro. Theo. Tech.,* vol. MTT-32, no. 5, May 1984, pp. 491–498.

[53] W.R. Zimmerman, "Network analog of Maxwell's field equations in one and two dimensions," *IEEE Trans. Educ.,* vol. E-25, no. 1, Feb. 1982, pp. 4–9.

[54] P.B. Johns and M. O'Brien, "Use of the transmission-line modeling (t.l.m.) method to solve non-linear lumped networks," *Radio Electron. Engr.,* vol. 50, no. 1/2, Jan./Feb., 1980, pp. 59–70.

[55] J.W. Bandler, et al., "Transmission-line modeling and sensitivity evaluation for lumped network simulation and design in the time domain," *J. Franklin Inst.,* vol. 304, no. 1, 1971, pp. 15–23.

[56] C.R. Brewitt-Taylor and P.B. Johns, "On the construction and numerical solution of transmission line and lumped network models of Maxwell's equations," *Inter. J. Numer. Meth. Engr.,* vol. 15, 1980, pp. 13–30.

[57] P. Saguet and W.J.R. Hoefer, "The modeling of multiaxial discontinuities in quasi-planar structures with the modified TLM method," *Int. J. Num. Model.,* vol. 1, 1988, pp. 7–17.

[58] E.M. El-Sayed and M.N. Morsy, "Analysis of microwave ovens loaded with lossy process materials using the transmission-line matrix method," *Int. J. Num. Meth. Engr.,* vol. 20, 1984, pp. 2213–2220.

[59] N.G. Alexopoulos, "Integrated-circuit structures on anisotropic substrates," *IEEE Trans. Micro. Theo. Tech.,* vol. MTT-33, no. 10, Oct. 1985, pp. 847–881.

[60] S. Akhatarzad and P.B. Johns, "TLMRES-the TLM computer program for the analysis of microstrip resonators," *IEEE Trans. Micro. Theo. Tech.,* vol. 35, no. 1, Jan. 1987, pp. 60–61.

[61] P.B. Johns, "A simple explicit and unconditionally stable numerical routine for the solution of the diffusion equation," *Int. Jour. Numer. Methods Engr.,* vol. 11, 1977, pp. 1307–1328.

[62] P.B. Johns and G. Butler, "The consistency and accuracy of the TLM method for diffusion and its relationship to existing methods," *Int. Jour. Numer. Methods Engr.,* vol. 19, 1983, pp. 1549–1554.

[63] P.W. Webb, "Simulation of thermal diffusion in transistors using transmission line matrix modeling," *Electron. Comm. Engr. Jour.,* vol. 4, no. 6, Dec. 1992, pp. 362–366.

[64] P. Naylor, C. Christopoulos, and P.B. Johns, "Coupling between electromagnetic field and wires using transmission-line modeling," *IEEE Proc.,* Pt. A, vol. 134, no. 8, 1987, pp. 679–686.

[65] P. Naylor and C. Christopoulos, "A new wire node for modeling thin wires in electromagnetic field problems solved by transmission line modeling," *IEEE Trans. Micro. Theo. Tech.,* vol. 38, no. 3, March 1990, pp. 328–330.

[66] J.A. Porti et al., "Comparison of the thin-wire models for TLM method," *Elect. Lett.,* vol. 28, no. 20, Sept. 1992, pp. 1910–1911.

[67] A.P. Duffy et al., "New methods for accurate modeling of wires using TLM," *Elect. Lett.,* vol. 29, no. 2, Jan. 1993, pp. 224–226.

[68] I. Palocz and N. Marcovitz, "A network-oriented approach in the teaching of electromagnetics," *IEEE Trans. Educ.,* vol. E-28, no. 3, Aug. 1985, pp. 150–154.

[69] H. Pues and A. Van de Capelle, "Accurate transmission-line model for the rectangular microstrip antenna," *IEEE Proc.,* vol. 131, Pt. H, no. 6, Dec. 1984, pp. 334–340.

[70] J.F. Deford and O.P. Gandhi, "An impedance method to calculate currents induced in biological bodies exposed to quasi-static electromagnetic fields," *IEEE Trans. Elect. Comp.,* vol. EMC-27, no. 3, Aug. 1985, pp. 168–173.

[71] D.A. Al-Mukhtar and T.E. Sitch, "Transmission-line matrix method with irregularly graded space," *IEEE Proc.,* vol. 128, Pt. H, no. 6, Dec. 1981, pp. 299–305.

[72] H.L. Thal, Exact circuit analysis of spherical waves," *IEEE Trans. Ant. Prog.,* vol. AP-26, no. 2, Mar. 1978, pp. 282–287.

[73] C.V. Jones and D.L. Prior, "Unification of fields and circuit theories of electrical machines," *Proc. IEEE,* vol. 119, no. 7, July 1972, pp. 871–876.

[74] P. Hammond and G.J. Rogers, "Use of equivalent circuits in electrical-machine studies," *Proc. IEEE,* vol. 121, no. 6, June 1974, pp. 500–507.

[75] E.M. Freeman, "Equivalent circuits from electromagnetic theory: low-frequency induction devices," *Proc. IEEE,* vol. 121, no. 10, Oct. 1974, pp. 1117–1121.

[76] W.J. Karplus and W.W. Soroka, *Analog Methods: Computation and Simulation.* New York: McGraw-Hill, 1959.

[77] G.L. Ragan (ed.), *Microwave Transmission Circuits.* New York: McGraw-Hill, 1948, pp. 544–547.

[78] R.H. MacNeal, *Electric Circuit Analogies for Elastic Structures,* vol. 2. New York: John Wiley & Sons, 1962.

[79] S. Akhtarzad, "Analysis of lossy microwave structures and microstrip resonators by the TLM method," Ph.D. thesis, University of Nottingham, England, July 1975.

[80] P.B. Johns, "On the relationship between TLM and finite-difference methods for Maxwell's equations," *IEEE Trans. Micro. Theo. Tech.,* vol. MTT-35, no. 1, Jan. 1987, pp. 60, 61.

[81] D.H. Choi and W.J.R. Hoefer, "The finite-difference time-domain method and its application to eingenvalue problems," *IEEE Trans. Micro. Theo. Tech.,* vol. 34, no. 12, Dec. 1986, pp. 1464–1472.

[82] D.H. Choi, "A comparison of the dispersion characteristics associated with the TLM and FD-TD methods," *Int. Jour. Num. Model.,* vol. 2, 1989, pp. 203–214.

[83] Z. Chen, M. Ney, and W.J.R. Hoefer, "A new finite-difference time-domain formulation and its equivalence with the TLM symmetrical condensed node," *IEEE Trans. Micro. Theo. Tech.,* vol. 39, no. 12, Dec. 1992, pp. 2160–2169.

[84] M. Krumpholz and P. Russer, "Two-dimensional FDTD and TLM," *Int. Jour. Num. Model.,* vol. 7, no. 2, 1994, pp. 141–143.

[85] M. Krumpholz and P. Russer, "On the dispersion of TLM and FDTD," *IEEE Trans. Micro. Theo. Tech.,* vol. 42, no. 7, July 1994, pp. 1275–1279.

[86] M. Krumpholz, C. Huber, and P. Russer, "A field theoretical comparison of FDTD and TLM," *IEEE Trans. Micro. Theo. Tech.,* vol. 43, no. 8, Aug. 1995, pp. 1935–1950.

Problems

7.1 Verify Eq. (7.16).

7.2 For the two-port network in Fig. 7.30 (a), the relation between the input and output variables can be written in matrix form as

$$\begin{bmatrix} V_1 \\ I_1 \end{bmatrix} = \begin{bmatrix} A & B \\ C & D \end{bmatrix} \begin{bmatrix} V_2 \\ -I_2 \end{bmatrix}$$

For the lossy line in Fig. 7.30 (b), show that the ABCD matrix (also called the cascaded matrix) is

$$\begin{bmatrix} \cosh \gamma \ell & Z_o \sinh \gamma \ell \\ \frac{1}{Z_0} \sinh \gamma \ell & \cosh \gamma \ell \end{bmatrix}$$

7.3 The circuit in Fig. 7.31 is used to model diffusion processes and presents a Δz section of a lossy transmission line. Show that

$$\frac{\partial^2 V}{\partial z^2} = -Ri + RC \frac{\partial V}{\partial t} - L \frac{\partial i}{\partial t} + LC \frac{\partial^2 V}{\partial t^2}$$

where $i = I_m / \Delta z$, the current density.
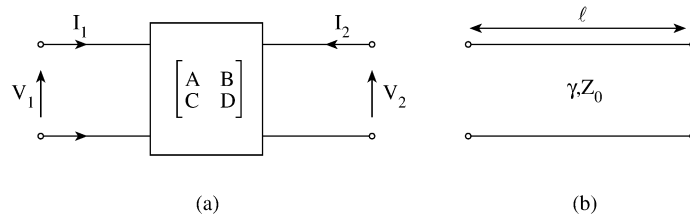
Figure 7.30
For Problem 7.2.
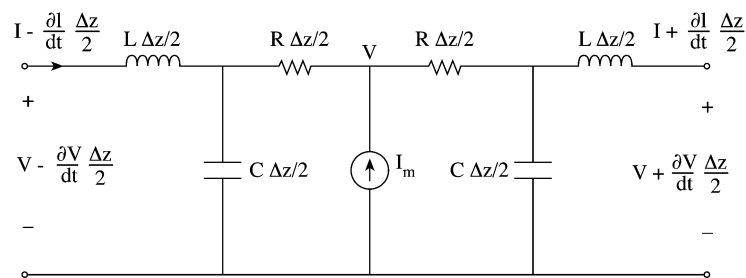
Figure 7.31
For Problem 7.3.

7.4 Consider an EM wave propagation in a lossless medium in TEM mode ($E_y = 0 = E_z = H_z = H_x$) along the z direction. Using one-dimensional TLM mesh, derive the equivalencies between network and field quantities.

7.5 Modify the program in Fig. 7.14 to calculate the cutoff frequency (expressed in terms of $\Delta \ell / \lambda$) in a square section waveguide of size $10\Delta \ell$. Perform the calculation for the TM_{11} mode by using open-circuit symmetry boundaries to suppress even-order modes and by taking the excitation and output points as in Fig. 7.32 to suppress the TM_{13}, TM_{33}, and TM_{15} modes. Use $N = 500$.

7.6 Repeat Prob. 7.5 of higher-order modes but take excitation and output points as in Fig. 7.33.

7.7 For the waveguide with a free space discontinuity considered in Example 7.2, plot the variation of the magnitude of the normalized impedance of the guide with $\Delta \ell / \lambda$. The plot should be for frequencies above and below the cutoff frequency, i.e., including both evanescent and propagating modes.

7.8 Rework Example 7.5, but take the output point at $(x = 6, z = 13)$.

7.9 Verify Eq. (7.62).

——— Short circuit boundary
----- Open circuit boundary
○　　　Source point
×　　　Output point
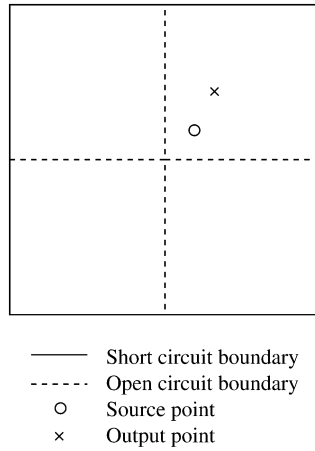
Figure 7.32
Square cross section waveguide of Problem 7.4.

——— Short circuit boundary
○　　　Source point
×　　　Output point
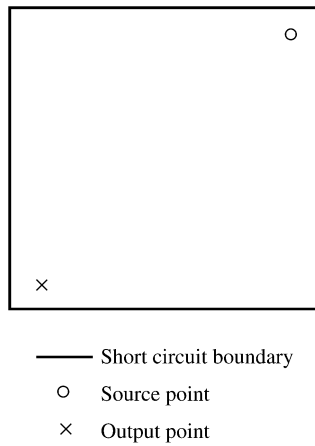
Figure 7.33
Square cross section waveguide of Problem 7.6.

7.10 For transverse waves on a stub-loaded transmission-line matrix, the dispersion relation is given by

$$\sin^2\left(\frac{\beta_n \Delta\ell}{2}\right) = 2\,(1 + Y_o/4)\sin^2\left(\frac{\omega\Delta\ell}{2c}\right)$$

Plot the velocity characteristic similar to that in Fig. 7.11 for $Y_o = 0$, 1, 2, 10, 20, 100.

7.11 Verify Eq. (7.68).

7.12 The transmission equation for one cell in a stub-loaded three-dimensional TLM network is

$$\begin{bmatrix} V_i \\ I_i \end{bmatrix} = T \cdot \begin{bmatrix} 1 & j(2+z_o)\tan\theta/2 \\ 0 & 1 \end{bmatrix} \cdot T \cdot T \cdot \begin{bmatrix} 1 & 0 \\ g_o + j(2+y_o)\tan\theta/2 & 1 \end{bmatrix} \cdot T \cdot \begin{bmatrix} V_{i+1} \\ I_{i+1} \end{bmatrix}$$

where

$$T = \begin{bmatrix} \cos\theta/4 & j\sin\theta/4 \\ j\sin\theta/4 & \cos\theta/4 \end{bmatrix}$$

$\theta = 2\pi\Delta\ell/\lambda$, $y_o = 4(\epsilon_r - 1)$, $z_o = 4(\mu_r - 1)$, and $g_o = \sigma\Delta\ell\sqrt{L/C}$. Assuming small losses $\alpha_n\Delta\ell \ll 1$, show that the transmission equation can be reduced to

$$\begin{bmatrix} V_i \\ I_i \end{bmatrix} = \begin{bmatrix} e^{\gamma_n\Delta\ell} & 0 \\ 0 & e^{\gamma_n\Delta\ell} \end{bmatrix} \begin{bmatrix} V_{i+1} \\ I_{i+1} \end{bmatrix}$$

where $\gamma_n = \alpha_n + j\beta_n$ is the propagation constant and

$$\cos(\beta_n\Delta\ell) = 1 - 8(1+y_o/4)(1+z_o/4)\sin^2\theta/2$$

$$\alpha_n\Delta\ell\sin(\beta_n\Delta\ell) = \frac{g_o}{2}(4+z_o)\sin\theta/2\cos\theta/2$$

7.13 In the y-z plane of a symmetric condensed node of the TLM mesh, the normalized characteristic impedance of the inductive stub is

$$Z_x = \frac{2\mu_r}{u_o\Delta t} \cdot \frac{\Delta y\Delta z}{\Delta x} - 4$$

Assuming that $\Delta x = \Delta y = \Delta z = 0.1$ m, determine the stubs required to model a medium with $\epsilon_r = 4$, $\mu_r = 1$, $u_o = c$, and the value of Δt for stability.

7.14 Consider the 61×8 rectangular matrix with boundaries at $x = 0.5$ and $x = 8.5$ as in Fig. 7.34. By making one of the boundaries, say $x = 8.5$, an open circuit, a waveguide of twice the width can be simulated. For the TE_{m0} family of modes, excite the system at all points on line $z = 1$ with impulses corresponding to E_y and take the impulse function of the output at point $x = 7$, $z = 6$. Calculate the normalized wave impedance $Z = E_y/H_x$ for frequencies above cutoff, i.e., $\Delta\ell/\lambda = 0.023, 0.025, 0.027, \ldots, 0.041$. Take $\sigma = 0$, $\epsilon_r = 2$, $\mu_r = 1$.

7.15 Repeat Prob. 7.14 for a lossy waveguide with $\sigma = 278$ mhos/m, $\epsilon_r = 1$, $\mu_r = 1$.

7.16 Using the TLM method, determine the cutoff frequency (expressed in terms of $\Delta\ell/\lambda$) of the lowest order TE and TM modes for the square waveguide with cross section shown in Fig. 7.35. Take $\epsilon_r = 2.45$.

7.17 For the dielectric ridge waveguide of Fig. 7.36, use the TLM method to calculated the cutoff wavenumber k_c of the dominant mode. Express the result in terms of $k_c a(= \omega a/c)$ and try $\epsilon_r = 2$ and $\epsilon_r = 8$. Take $a = 10\Delta\ell$.
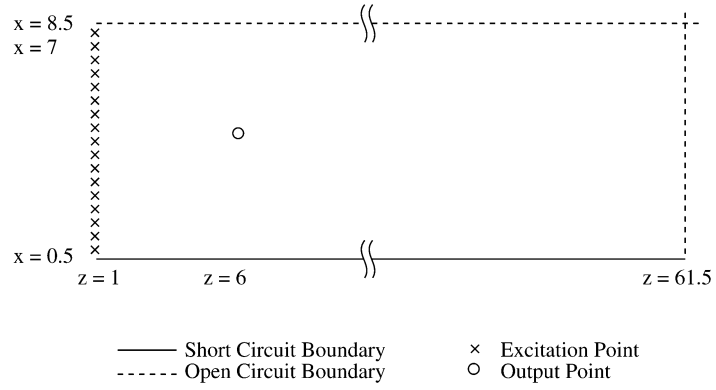
Figure 7.34
The 61×8 TLM mesh of Problem 7.14.
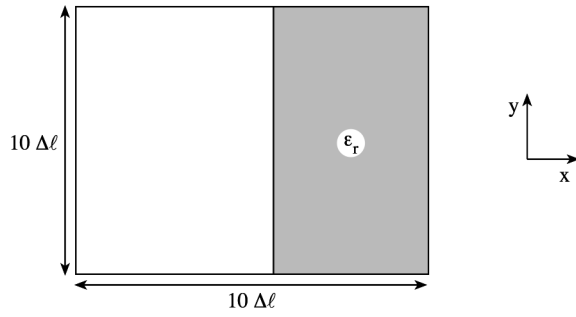
Figure 7.35
For Problem 7.16.
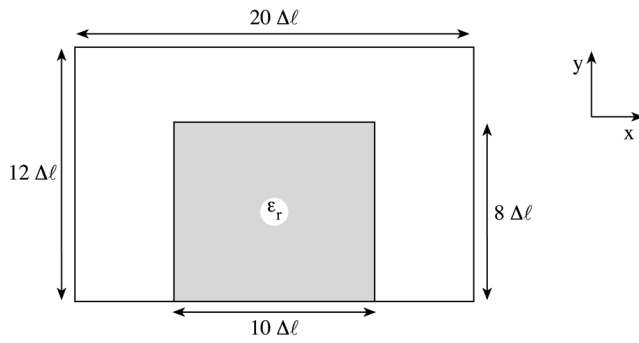
Figure 7.36
For Problem 7.17.

7.18 Rework Example 7.6 for the inhomogeneous cavity of Fig. 7.37. Take $\epsilon_r = 16$, $a = 12\Delta\ell$, $b = 3a/10$, $d = 4a/10$, $s = 7a/12$, $u = 3d/8$.
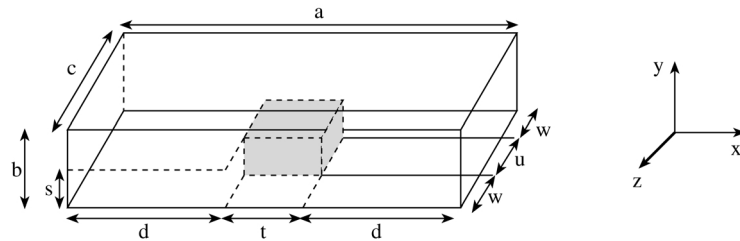

Figure 7.37

The inhomogeneous cavity of Problem 7.18.

7.19 Consider a single microstrip line whose cross section is shown in Fig. 7.38. Dispersion analysis of the line by the TLM method involves resonating a section
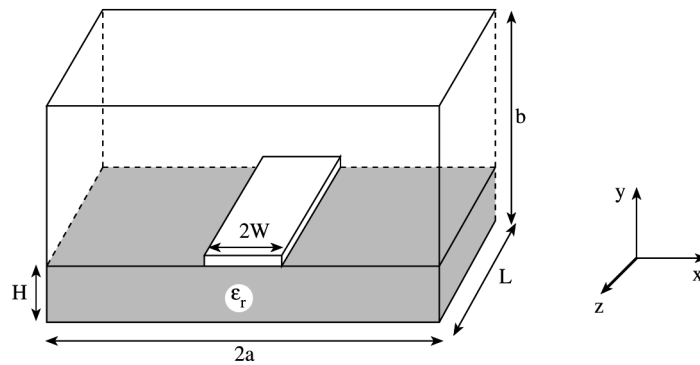

Figure 7.38

The microstrip line of Problem 7.19.

of the transmission line by placing shorting planes along the axis of propagation (the z-axis in this case). Write a TLM computer program and specify the input data as:

$$E_x = 0 = E_z \text{ along } y = 0, \ y = b,$$
$$E_x = 0 = E_z \text{ along } x = 2a,$$
$$E_x = 0 = E_z \text{ for } y = H, \ -W \le x \le W,$$
$$H_y = 0 = H_z \text{ along } x = 0$$

Plot the dispersion curves depicting the phase constant β as a function of frequency f for cases when the line is air-filled and dielectric-filled. The distance $L(= \pi/\beta)$ between the shorting planes is the variable. Assume the dielectric

substrate and the walls of the enclosure are lossless. Take $\epsilon_r = 4.0$, $a = 2$ mm, $H = 1.0$ mm, $W = 1.0$ mm, $b = 2$ mm, $\Delta\ell = a/8$.

7.20 For the cubical cavity of Fig. 7.39, use the TLM technique to calculate the time taken for the total power in the lossy dielectric cavity to decay to $1/e$ of its original value. Consider cases when the cavity is completely filled with dielectric material and half-filled. Take $\epsilon_r = 2.45$, $\sigma = 0.884$ mhos/m, $\mu_r = 1$, $\Delta\ell = 0.3$ cm, $2a = 7\Delta\ell$.
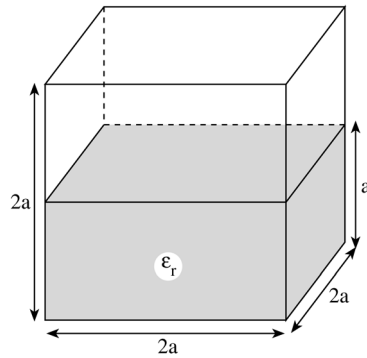

Figure 7.39
The lossy cavity of Problem 7.20.